DIPLOMARBEIT

Spectroscopy of the $6S_{1/2} \to 5D_{5/2}$ Electric Quadrupole Transition of Atomic Cesium

zur Erlangung des akademischen Grades

Diplom-Ingenieur

im Rahmen des Studiums

Masterstudium Technische Physik

eingereicht von

Sebastian Pucher

Matrikelnummer 01129824

ausgeführt am Atominstitut
der Fakultät für Physik der Technischen Universität Wien

Betreuung
Betreuer: Univ.Prof. Dr. Arno Rauschenbeutel
Mitwirkung: Dr. Alexandre Dareau, Dr. Philipp Schneeweiss, Dr. Christoph Clausen

Wien, 10.09.2018   _____   _____
                        (Unterschrift Verfasser)   (Unterschrift Betreuer)

Contents

Abstract

The $6S_{1/2} \to 5D_{5/2}$ electric quadrupole transition of cesium is studied experimentally via Doppler-free spectroscopy in a hot vapor. With a three-level coupled system, the hyperfine structure of this transition is resolved. The intensities of the lines in the spectrum are investigated and the optical pumping dynamics are analyzed. Furthermore, a laser is stabilized to the $6S_{1/2} \to 5D_{5/2}$ transition. This makes the presented setup a useful tool for further investigations of electric quadrupole transitions. Based on our results, we plan future experiments with laser-cooled atoms close to surfaces, e.g., to enhance the quadrupole coupling.

List of Abbreviations

AM   amplitude modulation

AOM   acousto-optic modulator

DC   direct current

E1   electric dipole

E2   electric quadrupole

FM   frequency modulation

FWHM   full width at half maximum

λ wavelength

LO   local oscillator

MOT   magneto-optical trap

PI   proportional and integral

PID   proportional, integral, and derivative

RF   radio frequency

rms   root-mean-square

SPCM   single photon counting module

TTL   transistor-transistor logic

Introduction

High-resolution spectroscopy with lasers is an important tool in atomic and molecular physics. Experiments in this field set new standards in modern-day metrology and provide unique possibilities for studying atomic and molecular structures in detail. High-resolution spectra can also serve as an absolute frequency reference or can be used to stabilize lasers. These lasers can then be used for further tasks.

A common method to obtain high-resolution spectra is nonlinear Doppler-free laser spectroscopy. In atomic physics, such spectroscopy methods have been used mainly to study electric dipole (E1) transitions. However, in recent years, E1 forbidden transitions have been garnering attention. Electric quadrupole (E2) transitions which are being driven by field gradients of optical beams, in particular, became interesting because they can occur even where there is no light intensity at the center-of-mass position of the atom, but only a field gradient [1, 2]. These E2 transitions are typically weaker than E1-allowed transitions, however, the electric quadrupole interaction can be enhanced by tailoring the laser field [3–5].

Spectroscopy of E2 transitions in a vapor cell is affected by Doppler broadening [6, 7], but several methods have been used to investigate the hyperfine lines of such transitions in cesium [8, 9] and rubidium [10, 11]. In this thesis, we utilize three-level Raman-type nonlinear spectroscopy [9, 12–14] to study the hyperfine lines of the $6S_{1/2} - 5D_{5/2}$ E2 transition in a hot cesium vapor cell. We use the $6S_{1/2}$, $6P_{3/2}$, and the $5D_{5/2}$ states to resolve the hyperfine structure of the E2 transition, similar to [9].

This thesis was done in the Rauschenbeutel group at the Atominstitut of TU Wien. This research group performs experiments with laser-cooled cesium atoms optically trapped in the vicinity of optical nanofibers [15]. An attractive wavelength for trapping is around 687 nm because the differential AC Stark shifts for $6S_{1/2}$ and $6P_{3/2}$ states cancel [16]. The $6S_{1/2} \rightarrow 5D_{5/2}$ E2 transition has a wavelength of about 685 nm which is close to the trapping wavelength at 687 nm. The present work can help to study the E2 transition close to nanofibers and to investigate the effects on the trapping performances. The evanescent field around the nanofiber could be used to enhance the E2 transition and to study these transitions in a strong field gradient around the nanofiber [17].

The first chapter of this thesis consists of the theoretical background of E2 transition and three-level Doppler-free spectroscopy. The second chapter presents the experimen-

tal setups used for the measurements in this thesis. In the last chapter, we show and discuss the measurements of the hyperfine lines of the $6S_{1/2} - 5D_{5/2}$ E2 transition.

Chapter 1

Theoretical Framework

In this section, we discuss the theory relevant for this thesis. The first part deals with optical transitions of multi-level atoms. We will discuss the electric dipole approximation, then we will extend this approximation to describe E2 transitions. Afterward, we will present the investigated level scheme of cesium and discuss the E2 transition of this scheme in more detail. The second part discusses the Doppler-free spectroscopy methods used in this thesis.

1.1 Optical Transitions

In this thesis, we study the transition between the $6S_{1/2}$ electronic ground state and the $5D_{5/2}$ state of cesium. This transition has a wavelength of $\lambda = 685\,\mathrm{nm}$. Because the orbital momentum quantum number l is changing by $+2$, this transition is forbidden by the selection rules of the electric dipole term, but it is allowed for higher-order light-matter coupling, considering the electric quadrupole term. In this section, we discuss the electric dipole approximation and the extension in order to get to the electric quadrupole selection rules.

1.1.1 Electric Dipole Approximation

With the Hamiltonian $\mathcal{H}(t)$ and the wavefunction $\Psi(t)$, we can write the time-dependent Schrödinger equation as

$$\mathcal{H}(t)\Psi(t) = i\hbar\frac{\partial\Psi(t)}{\partial t}. \tag{1.1}$$

When an atom is exposed to radiation, $\mathcal{H}(t)$ can be written as a combination of the Hamiltonian of a free atom $\mathcal{H}_0 = \frac{p_{\mathrm{kin}}^2}{2m} + V(r)$ and a time-dependent interaction Hamiltonian $\mathcal{H}'(t)$. In this section, we will derive an expression for $\mathcal{H}'(t)$ and discuss the resulting transition amplitudes.

In the Hamiltonian $\mathcal{H}(t) = \mathcal{H}_0 + \mathcal{H}'(t)$, the kinetic momentum $\boldsymbol{p}_{\mathrm{kin}}$ is included, but the Lagrange and Hamilton formalism in electrodynamics states that this momentum is no longer equal to the kinetic momentum $\boldsymbol{p}_{kin} = m\boldsymbol{v}$ if an electromagnetic vector

potential $\boldsymbol{\mathcal{A}}$ is present [18]. Instead, the time-dependent field momentum $e\boldsymbol{\mathcal{A}}(t)$ must be added where e is the charge of an electron. This gives the total momentum

$$\boldsymbol{p} = \boldsymbol{p}_{kin} + e\boldsymbol{\mathcal{A}}(\boldsymbol{r}, t), \tag{1.2}$$

which is also known as the conjugate momentum. The Hamiltonian for the valence electron of an atom in an electro-magnetic field is therefore

$$\mathcal{H}(t) = \frac{1}{2m}(\boldsymbol{p} - e\boldsymbol{\mathcal{A}}(\boldsymbol{r}, t))^2 + V(\boldsymbol{r}) - eU(\boldsymbol{r}, t), \tag{1.3}$$

where $V(\boldsymbol{r})$ is the electrostatic potential due to the interaction with the nucleus and the other electrons, $U(\boldsymbol{r}, t)$ is the scalar potential of the external field and $\boldsymbol{p}$ and $\boldsymbol{\mathcal{A}}(\boldsymbol{r}, t)$ are operators which may not necessarily commute. However, in the Coulomb gauge, where $\boldsymbol{\nabla} \cdot \boldsymbol{\mathcal{A}}(t) = 0$, the operators commute when we consider the product rule. Therefore we can write $\boldsymbol{p} \cdot \boldsymbol{\mathcal{A}}(t) + \boldsymbol{\mathcal{A}}(t) \cdot \boldsymbol{p} = 2\boldsymbol{\mathcal{A}}(t) \cdot \boldsymbol{p}$, and expand the term in the parentheses. The $|\boldsymbol{\mathcal{A}}(t)|^2$ term can be neglected for small light-matter coupling strengths. Thus the Hamiltonian becomes

$$\mathcal{H}(t) = \frac{\boldsymbol{p}^2}{2m} + V(r) + \frac{e\boldsymbol{\mathcal{A}}(\boldsymbol{r}, t) \cdot \boldsymbol{p}}{m} - eU(\boldsymbol{r}, t) = \mathcal{H}_0 + \mathcal{H}'(t). \tag{1.4}$$

In the Coulomb gauge, $U(\boldsymbol{r}, t)$ vanishes and the external electric field only gives a contribution to $\boldsymbol{\mathcal{A}}(\boldsymbol{r}, t)$. For an atom at the origin, we can write

$$\boldsymbol{\mathcal{A}}(\boldsymbol{r}, t) = \boldsymbol{\mathcal{A}}_0(0, t) \exp[i\boldsymbol{k} \cdot \boldsymbol{r} - \omega t] + c.c., \tag{1.5}$$

where $\boldsymbol{k}$ is the wave vector, $\omega = ck$ is the angular frequency of the light field, c.c. is the complex conjugate, and $\boldsymbol{\mathcal{A}}_0$ is the amplitude of the wave which defines its polarization. The dipole approximation assumes that the external field does not change over the volume of the atom. This is a reasonable assumption because the Bohr radius $a_0 \approx 0.5\,\text{Å}$ is small compared to the optical wavelength $\lambda \approx 500\,\text{nm}$ which means that $\boldsymbol{k} \cdot \boldsymbol{r} \ll 1$. We can expand $\boldsymbol{\mathcal{A}}(\boldsymbol{r}, t)$

$$\boldsymbol{\mathcal{A}}(\boldsymbol{r}, t) = \boldsymbol{\mathcal{A}}_0(0, t)(1 + i\boldsymbol{k} \cdot \boldsymbol{r} + \mathcal{O}(\boldsymbol{k} \cdot \boldsymbol{r})^2), \tag{1.6}$$

and, in dipole approximation, we neglect higher order terms and consider only the zeroth order to find $\boldsymbol{\mathcal{A}}(\boldsymbol{r}, t) \approx \boldsymbol{\mathcal{A}}_0(0, t)$.

The transition rate between two states $|\psi_i\rangle$ and $|\psi_f\rangle$ is proportional to the square of the transition matrix element $\mathcal{M}_{if}(t)$, defined as [18]

$$\mathcal{M}_{if}(t) = \langle\psi_f| \mathcal{H}'(t) |\psi_i\rangle = \boldsymbol{\mathcal{A}}_0(t) \cdot \langle\psi_f| \boldsymbol{p} |\psi_i\rangle, \tag{1.7}$$

where the wave functions ψ_f and ψ_i of a state i and a state f are defined by the quantum numbers of the unperturbed atom. We can use the Heisenberg picture to transform the interaction $\boldsymbol{A} \cdot \boldsymbol{p}$ into the electric dipole interaction $\boldsymbol{\mu} \cdot \boldsymbol{E}$ where $\boldsymbol{\mu}$ is the electric dipole moment defined by $\boldsymbol{\mu} = -e\boldsymbol{r}$ and $\boldsymbol{E}$ is the external electric field [19]. For $\mathcal{M}_{if}(t)$, it is therefore also common to write

$$\mathcal{M}_{if}(t) = \langle \psi_f | \, \boldsymbol{\mu} \cdot \boldsymbol{E} \, | \psi_i \rangle . \tag{1.8}$$

If these matrix elements are evaluated, it turns out that only transitions involving specific changes in the quantum numbers are possible. These dipole selection rules are presented in table 1.1 in section 1.1.3. For all other combinations of quantum numbers, the matrix element vanishes and the transition is called dipole-forbidden. In particular, the matrix element disappears for $\Delta l = +2$ which is the case for the transition $6S_{1/2} \rightarrow 5D_{5/2}$.

1.1.2 Electric Quadrupole Approximation

Equation 1.8 defines selection rules for dipole-allowed transitions. However, measurements show that it is possible to observe dipole-forbidden transitions which do not satisfy these rules. This is the case for the $6S_{1/2} \rightarrow 5D_{5/2}$ transition that we study here. To understand such transitions, we have to go beyond the dipole approximation. This means that $i\boldsymbol{k} \cdot \boldsymbol{r}$ term in equation 1.6 cannot be neglected. When we consider the next order, we take two terms into account. The first term arises from the magnetic moments produced by moving charges within an atom and the second term comes from the quadrupole moment of the charge distribution induced by the light field. We can add both terms to the interaction Hamiltonian [19]

$$\mathcal{H}'_{(2)} = -\boldsymbol{\mu}^E \cdot \boldsymbol{E} - \boldsymbol{\mu}^B \cdot \boldsymbol{B} - \sum_{ij} Q_{ij} \nabla_i E_j, \tag{1.9}$$

where $\boldsymbol{\mu}^B$ is the magnetic dipole moment, Q_{ij} is the electric quadrupole moment, and $\nabla_i E_j$ are the spatial derivatives of the electric field components E_j. This electric quadrupole tensor is defined as [17]

$$Q_{ij} = e(3x_i x_j - R^2 \delta_{ij}), \tag{1.10}$$

where δ_{ij} is the Kronecker delta, x_i is the ith coordinate of the valence electron, and $R = \sqrt{x_1^2 + x_2^2 + x_3^2}$. The magnetic dipole moment interacts with the external magnetic field $\boldsymbol{B}$ with approximately the same strength as the electric quadrupole moment interacts with the electric field gradient $\nabla_i E_j$. Because the magnetic dipole and electric quadrupole moments arise from the $i\boldsymbol{k} \cdot \boldsymbol{r}$ term in equation 1.6, the rate of these

Table 1.1: Selection rules for electric dipole (E1) and electric quadrupole (E2) transitions [17, 19, 20].

	E1	E2
Δl	± 1	$0, \pm 2$
ΔJ	$0, \pm 1$ $J = 0 \not\leftrightarrow 0$	$0, \pm 1, \pm 2$ $J = 0 \not\leftrightarrow 0, 0 \not\leftrightarrow 1, \frac{1}{2} \not\leftrightarrow \frac{1}{2}$
ΔM_J	$0, \pm 1$ $M_J = 0 \not\leftrightarrow 0$ if $\Delta J = 0$	$0, \pm 1, \pm 2$
ΔF	$0, \pm 1$ $F = 0 \not\leftrightarrow 0$	$0, \pm 1, \pm 2$ $F = 0 \not\leftrightarrow 0, 0 \not\leftrightarrow 1, \frac{1}{2} \not\leftrightarrow \frac{1}{2}$

transitions relative to the E1 transitions can be estimated as [19]

$$(\boldsymbol{k} \cdot \boldsymbol{r})^2 = \left(\frac{2\pi a_0}{\lambda}\right)^2 = \left(\frac{\hbar\omega}{m_e c^2 \alpha}\right)^2 \approx \frac{\alpha^2}{4} \approx 1.3 \cdot 10^{-5}, \qquad (1.11)$$

where c is the speed of light, m_e is the mass of the electron, $\alpha = \frac{e^2}{4\pi\epsilon_0 \hbar c}$ is the fine structure constant, and $a_0 = \frac{\hbar}{\alpha m_e c}$ is the Bohr radius of a hydrogen atom. Here, we used that the photon energy is equal to the energy separation of two levels

$$\hbar\omega = E_f - E_i = -\frac{m_e c^2 \alpha^2}{2}\left[\frac{1}{n_f^2} - \frac{1}{n_i^2}\right] \approx \frac{m_e c^2 \alpha^2}{2}, \qquad (1.12)$$

where n_i and $n_f = n_i + 1$ are the principal quantum numbers of the states ψ_i and ψ_f. Because of equation 1.11, the rates of the magnetic dipole and E2 transitions are typically five orders of magnitude smaller than those of the E1 transitions.

1.1.3   Electric Quadrupole Selection Rules

For a transition with $\Delta l = 0, \pm 2$, only the last term in the interaction Hamiltonian 1.9 is relevant, because the transition matrix elements of the other terms vanish. To find the electric quadrupole selection rules, we have to calculate the matrix elements

$$\langle \psi_f | Q_{ij} \nabla_i E_j | \psi_i \rangle \qquad (1.13)$$

with the quadrupole tensor operators Q_{ij}. The wavefunctions ψ_f and ψ_i are defined by the quantum numbers, and transitions are possible only for specific changes of these quantum numbers. In table 1.1, we summarized the possible changes of the orbital momentum quantum number l, the quantum number of the total angular momentum J, the projection of the total angular momentum M_J, and the the quantum number for the total angular momentum of the Atom F as a result of E2 transition selection rules.

We now want to discuss selection rules of E2 transitions in more detail. The selection
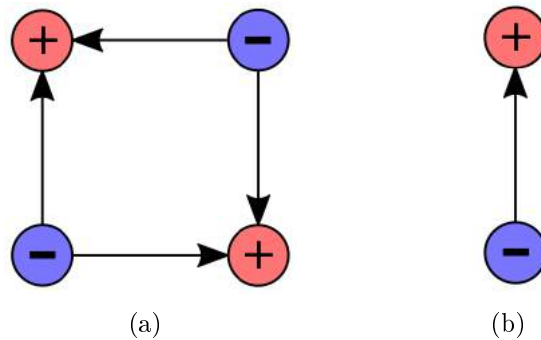
Figure 1: Illustration of (a) an electric quadrupole and (b) an electric dipole. The configuration of the poles explains the even parity of a quadrupole and the uneven parity of a dipole.

rule of the angular quantum number l can be understood geometrically. The electric quadrupole consists of alternating positive and negative charges which are arranged on the corners of a square as illustrated in figure 1(a). When we mirror a quadrupole at the origin, the charges keep their sign, in contrast to a dipole where the sign of the charges switch (figure 1(b)). This means that the parity of the wavefunctions of two states, between those of where an E2 transition is happening, must have the same parity. The parity of a wave function is given by $(-1)^l$. Therefore, Δl must be even for an E2 transition. Elaborate calculations show that the selection rule of l for an E2 transition is $\Delta l = 0, \pm 2$ [21].

When an atom absorbs electric quadrupole radiation, the radiation transfers an angular momentum of $|\Delta J| = 2\hbar$, instead of $1\hbar$ for electric dipole radiation, to the atom. Considering this, we can explain the selection rules of the total angular momentum J with vector diagrams [21] as shown in figure 2. The total angular momentum of the atom $\boldsymbol{F}$ is defined as the sum of the nuclear spin and the total angular momentum of the electron as we will discuss in the next section. The selection rules of F are the same as for J because we change only the state of the electron. It is also possible to derive the various selection rules from equation 1.13 by using the Wigner-Eckart theorem as described in [17].

1.1.4 Level Scheme of Cesium

This thesis deals with spectroscopy of cesium. We study only the stable isotope ^{133}Cs. Cesium has 55 electrons, but because it is an alkali metal, we can readily describe its physical and chemical properties by studying only the outermost electron. In the ground state, this electron is in the $6S_{1/2}$ state, but with, for example, inelastic collisions [22] or lasers [23] it can be excited in other states.

In figure 3, we present the level scheme of cesium which we investigate in this thesis. In this level scheme, three states are involved: the $6S_{1/2}$, the $6P_{3/2}$, and the $5D_{5/2}$ state. The first number in the definition of the states describes the principal quantum number
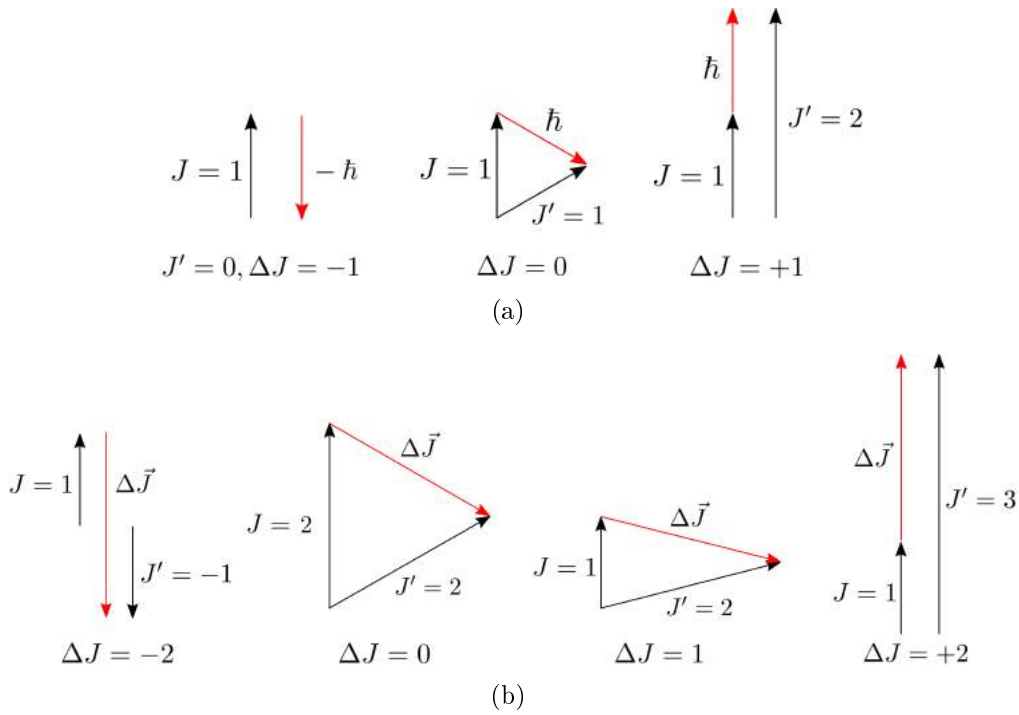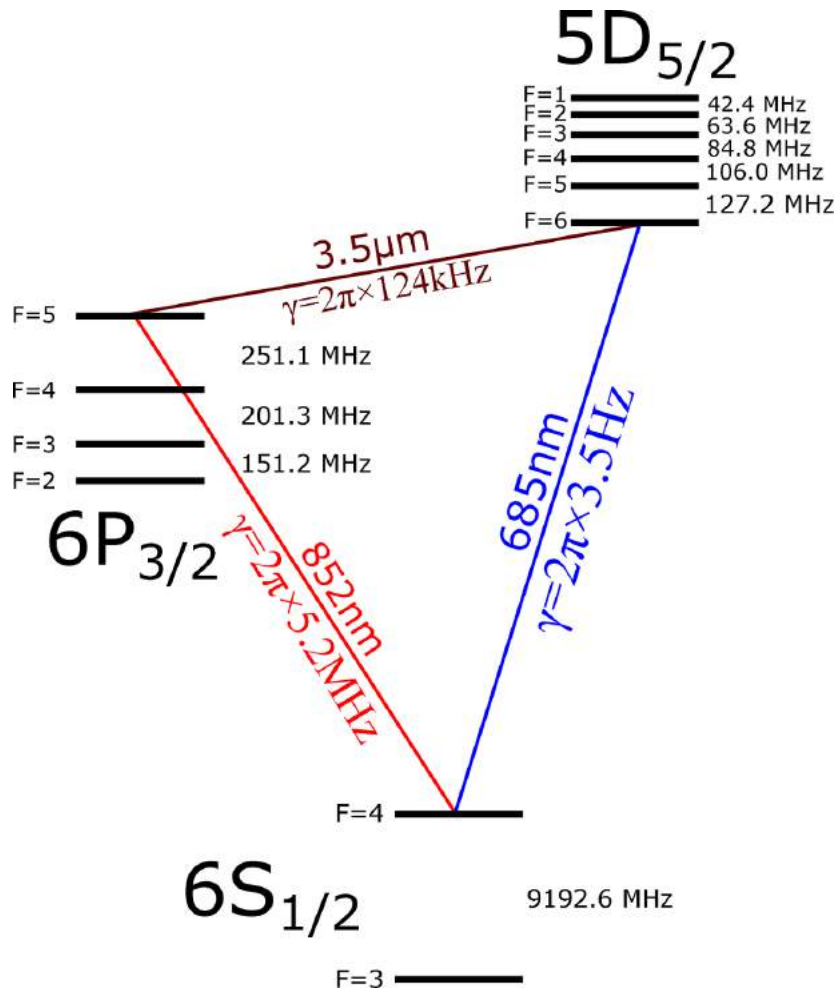
Figure 2: Vector diagrams which illustrate the selection rules of the total angular momentum J for (a) E1 transitions and (b) E2 transitions where the possible changes $\Delta J = J' - J$ are given by $|\Delta J| = \hbar$ and $|\Delta J| = 2\hbar$, respectively [21].

Figure 3: The level scheme of cesium which we investigate in this thesis.

n, the letter represents the total orbital angular momentum quantum number L, and the subscript is the value of the total angular momentum quantum number J. If the hyperfine structure of the states is relevant, we will write the total angular momentum quantum number F in parenthesis next to the other quantum numbers. For example, the $F = 4$ hyperfine level of the $6S_{1/2}$ state is denoted as $6S_{1/2}(F = 4)$.

The quantum number F describes the total angular momentum of the atom, given by

$$\hat{\boldsymbol{F}} = \hat{\boldsymbol{I}} + \hat{\boldsymbol{J}}, \tag{1.14}$$

where $\hat{\boldsymbol{I}}$ is the nuclear spin operator and $\hat{\boldsymbol{J}}$ is the operator of the total angular momentum of the electrons. F can have following values

$$F = |J - I|, |J - I| + 1, ..., J + I - 1, J + I. \tag{1.15}$$

This definition determines the number of hyperfine levels of every fine structure state. The nuclear spin of cesium is $I = \frac{7}{2}$. Therefore, the $6S_{1/2}$ state has two hyperfine levels, $F = 3$ and $F = 4$, the $6P_{3/2}$ state has four hyperfine levels, $F = 2, 3, 4, 5$, and the $5D_{5/2}$ state is split into six hyperfine levels, $F = 1, ..., 6$. The hyperfine levels of the $6S_{1/2}$ state are separated by a frequency of $9.192\,\text{GHz}$. This value is precisely known and the current definition of the second. Even in Doppler-broadened measurements, we can selectively excite cesium atoms either from the $F = 3$ or the $F = 4$ level to higher states because the separation between these levels is large compared to typical Doppler broadening at room temperature of about $500\,\text{MHz}$. The frequency spacing between the hyperfine levels of the $6P_{3/2}$ is smaller [24] and we cannot resolve them in Doppler-broadened measurements. However, there are several possibilities to measure these levels using Doppler-free spectroscopy. We discuss some of these Doppler-free methods in section 1.2. The same is true for the hyperfine levels of the $5D_{5/2}$ whose frequency separations are even smaller [25].

In the present level scheme, three transitions are possible (see figure 3). The transition between the $6S_{1/2}$ state and the $6P_{3/2}$ state is a dipole-allowed transition at a wavelength of about $\lambda = 852\,\text{nm}$. This transition is known as the D2 line of cesium and is very well investigated [26]. We excite atoms via the D2 line with a laser, which we will call the D2 laser in this thesis. The transition between the $6S_{1/2}$ state and the $5D_{5/2}$ state has a wavelength of about $\lambda = 685\,\text{nm}$ [27]. From the selection rules, we see that this is an E2 transition. We will call this transition the quadrupole line and the laser which drives this transition, quadrupole laser in this thesis. The third transition is between the $6P_{3/2}$ state and the $5D_{5/2}$ state. This E1 transition has a wavelength of about $\lambda = 3.5\,\text{µm}$ [28].

Because the E2 transition is dipole-forbidden, the decay rate of $\gamma_{5D6S} = 2\pi \times 3.5\,\text{Hz}$ [6] is very small compared to the decay rate of the D2 line which is about $\gamma_{6P6S} = 2\pi \times 5.22\,\text{MHz}$ [29]. Because of the low decay rate of the E2 transition, excited atoms

Table 1.2: Literature values of the wavelength and the frequency of the transitions which are investigated in this thesis.

Transition	Wavelength in air [nm]	Frequency [THz]
$6S_{1/2}(F = 4) - 5D_{5/2}$ [27]	684.89696(5)	437.59785(3)
$6S_{1/2}(F = 3) - 5D_{5/2}$ [27]	684.88233(5)	437.60720(3)
$6S_{1/2}(F = 4) - 6P_{3/2}(F = 5)$ [33]	852.12034530(1)	351.721960563(5)
$6S_{1/2}(F = 3) - 6P_{3/2}(F = 4)$ [33]	852.09868306(8)	351.730902117(34)

will mostly not decay directly back to the $6S_{1/2}$ ground state, but will rather decay to the $6P_{3/2}$ state because this E1 transition has a much higher decay rate of $\gamma_{5D6P} = 2\pi \times 124\,\mathrm{kHz}$ [23].

When atoms decay from the $5D_{5/2}$ state via the $6P_{3/2}$ state back to the ground state, two photons are emitted, the first at a wavelength of $\lambda = 3.5\,\mu\mathrm{m}$ and the second at a wavelength of $\lambda = 852\,\mathrm{nm}$. These photons are correlated and can be entangled [17, 30, 31]. It is possible to use these photons to measure the lifetime of the $5D_{5/2}$ state. Previous measurements have shown that the lifetime of this state is about $1.281\,\mu\mathrm{s}$ [23] which is very long compared to the lifetime of $30.55\,\mathrm{ns}$ of the $6P_{3/2}$ state [32].

1.1.5 $6S_{1/2} - 5D_{5/2}$ Transition of Cesium

In this thesis, we study the $6S_{1/2} - 5D_{5/2}$ E2 transition and the properties of the $5D_{5/2}$ state of cesium. Therefore, we want to take a closer look at this transition in this section. In the beginning, we present the literature value of the wavelength of this transition. Then, we determine the line strengths of the hyperfine transitions of the quadrupole line and calculate their saturation intensities.

Wavelength and Transition Rate

In Doppler-broadened measurements, two frequencies of the D2 line and the $6S_{1/2} \rightarrow 5D_{5/2}$ transition can be observed because of the large ground state hyperfine splitting of cesium. In [27], the wavelength in air of the $6S_{1/2}(F = 3, 4) \rightarrow 5D_{5/2}$ transitions have been determined. In table 1.2, these values are presented together with literature values of the D2 line [33].

In [6], the oscillator strength of the $6S_{1/2} \rightarrow 5D_{5/2}$ transition was determined to be $f_{ik} = (4.69 \pm 0.05) \times 10^{-7}$. We can convert that into a transition rate using [34]

$$\gamma_{ki} = \frac{2\pi e^2 \nu^2}{m_e c^3 \epsilon_0} \frac{g_i}{g_k} f_{ik}, \tag{1.16}$$

where ν is the frequency of the transition, e the elementary charge, ϵ_0 the electric constant, and the statistical weights are given by

$$g_{i(k)} = 2J_{i(k)} + 1. \tag{1.17}$$

Using a frequency of $\nu = 437.602\,41$ THz, we find a transition rate of the $6S_{1/2} \rightarrow 5D_{5/2}$ E2 transition of $\gamma_{5D6S} = 2\pi \times 3.536$ Hz. This is consistent with the value given in [9] and in the "NIST Atomic Spectra Database" [35].

Line Strength

We now want to discuss the line strength of transitions in our level scheme. Let us consider two states, connected through an E1 transition and which have a total angular momentum of J and J', respectively. When these states are split into hyperfine levels defined by F and F', we can calculate the line strengths with [26]

$$S_{FF'}^{D} = (2F' + 1)(2J + 1) \begin{Bmatrix} J & J' & 1 \\ F' & F & I \end{Bmatrix}^2,$$

$$(1.18)$$

where $I = 7/2$ is the nuclear spin of cesium and the curly brackets represent the Wigner's 6-j symbol. If the two states are connected via an E2 transition, we can calculate the relative intensities of the lines with [9,36]

$$S_{FF'}^{Q} = (2F' + 1)(2J + 1) \begin{Bmatrix} J & J' & 2 \\ F' & F & I \end{Bmatrix}^2.$$

$$(1.19)$$

We used this equation to calculate the relative line intensities between the $6S_{1/2}(F = 3, 4)$ state and the $5D_{5/2}(F' = 1 - 6)$ state. In figure 4(a), we present the line strengths when the ground state is the $6S_{1/2}(F = 3)$ level. The intensity and the frequency of the lines are plotted relative to the $5D_{5/2}(F' = 5)$ line. In figure 4(b), the ground state is the $6S_{1/2}(F = 4)$ state and we plotted intensity and frequency relative to the $5D_{5/2}(F' = 6)$ line.

Saturation Intensity

When a laser is near-resonant with an atomic transition and we increase the intensity of the laser, then the transition will saturate. This means for higher laser intensities, it is not possible to excite more atoms because stimulated emission causes atoms to decay back to the ground state. The saturation intensity I_{sat} depends on the total decay rate Γ of the optically excited state and the frequency ν and the decay rate to the lower state γ of the selected transition. We can define I_{sat} as [26]

$$\frac{I_{\text{sat}}}{I} = \frac{\Gamma^2}{2\Omega^2},$$
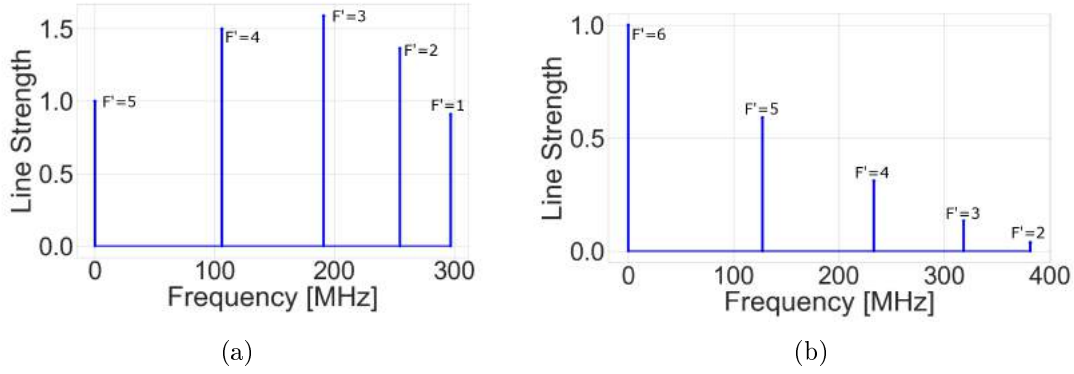
$$(1.20)$$

Figure 4: The calculated line intensities of the $6S_{1/2} \rightarrow 5D_{5/2}(F' = 1 - 6)$ hyperfine transitions. These line strengths corresponds to the expected line intensities when the atoms are excited (a) from the $6S_{1/2}(F = 3)$ level and (b) from the $6S_{1/2}(F = 4)$ level to the $5D_{5/2}$ state. Line strength and frequency are given relative to the hyperfine line with the highest F of the $5D_{5/2}$ state.

where Ω is the Rabi frequency of the transition. For an E1 transition, the resonant Rabi frequency Ω for arbitrary light polarization is

$$\Omega = - \langle \psi_f | \hat{\boldsymbol{\epsilon}} \cdot \boldsymbol{d} | \psi_i \rangle \frac{E_0}{\hbar}, \tag{1.21}$$

where $\hat{\boldsymbol{\epsilon}}$ is the unit polarization vector, $\boldsymbol{d}$ is the atomic dipole moment, and E_0 is the electric field amplitude at the position of the atom [37]. In the case of linearly polarized light ($\hat{\boldsymbol{\epsilon}} = \hat{\boldsymbol{z}}$), we can use this together with the intensity

$$I = \frac{\epsilon_0 c}{2} E_0^2 \tag{1.22}$$

to obtain the saturation intensity of an E1 transition

$$I_{\text{sat}} = \frac{c \epsilon_0 \hbar^2 \Gamma^2}{4 |\langle \psi_f | \hat{\boldsymbol{\epsilon}} \cdot \boldsymbol{d} | \psi_i \rangle|^2}. \tag{1.23}$$

We can eliminate the dipole matrix element with the relation [37]

$$\gamma = \frac{8\pi^2 \nu^3}{\epsilon_0 \hbar c^3} |\langle \psi_f | \boldsymbol{d}_z | \psi_i \rangle|^2 \tag{1.24}$$

which comes out of a full quantum electrodynamics calculation [37]. Here, ν is the frequency of the driving laser field and γ the decay rate of the transition driven with the laser. In a two level system, the decay rate of the upper state is $\Gamma = \gamma$ and, in this approximation, the saturation intensity of an E1 transition is

$$I_{\text{sat}} = \frac{2\pi^2 \hbar \nu^3 \gamma}{3c^2}. \tag{1.25}$$

In the level scheme of this thesis, three levels and an E2 transition are involved. The total decay rate of the upper state is the sum of the decay rates from the $5D_{5/2}$ state to the $6P_{3/2}$ state and to the $6S_{1/2}$ state, namely

$$\Gamma = \gamma_{5D6P} + \gamma_{5D6S}. \tag{1.26}$$

To calculate the saturation intensity of the quadrupole line, we also need its Rabi frequency. We now derive an expression of this Rabi frequency.

In the interaction picture and with rotating-wave approximation, the resonant Rabi frequency of an E2 transition is [17]

$$\Omega = \frac{1}{6\hbar} \sum_{ij} \langle \psi_f | \, Q_{ij} \, | \psi_i \rangle \frac{\partial E_i}{\partial x_j}, \tag{1.27}$$

where Q_{ij} is the electric quadrupole tensor. The atoms in the vapor cell are not prepared in a well-defined initial Zeeman state and there is no single Rabi frequency for a degenerate transition [38]. However, we can still define a rms Rabi frequency for a degenerate transition [17,38]

$$\bar{\Omega}^2_{FF'} = \frac{1}{2F+1} \sum_{MM'} |\Omega_{FMF'M'}|^2, \tag{1.28}$$

where $2F+1$ is a normalization factor as we have an incoherent mixture. When we assume that the electric wave is traveling in x-direction, we can write the electric field as a plane wave $\boldsymbol{E} = \boldsymbol{E_0} \exp[i(kx - \omega t)]$. Then, only the derivative with respect to x is nonzero. The squared derivative of the electric field is

$$|\frac{\partial \boldsymbol{E}}{\partial x}|^2 = |\boldsymbol{E_0} i k e^{i(kx - \omega t)}|^2 = \boldsymbol{E_0^2} |k|^2 = \boldsymbol{E_0^2} \frac{4\pi^2 \nu^2}{c^2}. \tag{1.29}$$

We use this to find the rms Rabi frequency [17]

$$\bar{\Omega}^2_{FF'} = \frac{e^2 \pi^2 \nu^2 |\boldsymbol{E_0}|^2}{10\hbar c^2 (2F+1)} |\langle n'F'||T^2||nF \rangle|^2, \tag{1.30}$$

where ν is the frequency of the transition and T^2 is a tensor operator which does not act on the nuclear spin degree of freedom. When we insert equation 1.22, equation 1.26, and equation 1.30 into equation 1.20, we obtain a saturation intensity of the quadrupole line of

$$I_{\text{sat}} = \frac{I\Gamma^2}{\bar{\Omega}^2_{FF'}} = \frac{10(2F+1)\hbar^2 c^3 \epsilon_0 \Gamma^2}{4\pi^2 e^2 \nu^2 |\langle n'F'||T^2||nF \rangle|^2}. \tag{1.31}$$

Table 1.3: Calculated saturation intensities of the different $6S_{1/2}(F) \to 5D_{5/2}(F')$ E2 hyperfine transitions. All values are given in W/cm^2.

				F'			
		1	2	3	4	5	6
F	3	1.89	1.26	1.08	1.15	1.72	
	4		14.60	4.17	1.80	0.95	0.56

The reduced matrix element $\langle n'F'||T^2||nF\rangle$ can be expressed as [17,39]

$$\langle n'F'||T^2||nF\rangle = (-1)^{J'+I+F}\sqrt{(2F+1)(2F'+1)}\begin{Bmatrix} F' & 2 & F \\ J & I & J' \end{Bmatrix}\langle n'J'||T^2||nJ\rangle. \tag{1.32}$$

Since the tensor operator T^2 does not act on the electron spin degree of freedom, we can write [17,39]

$$\langle n'J'||T^2||nJ\rangle = (-1)^{L'+S+J}\sqrt{(2J+1)(2J'+1)}\begin{Bmatrix} J' & 2 & J \\ L & S & L' \end{Bmatrix}\langle n'L'||T^2||nL\rangle. \tag{1.33}$$

In our case, the quantum numbers for the total angular momentum of the lower state and upper state are $L = 0$ and $L =' 2$, respectively. This yields a reduced matrix element of [17]

$$\langle n', L'=2||T^2||n, L=0\rangle = \sqrt{\frac{2}{3}}\langle n'=5, L'=2||r^2||n=6, L=0\rangle$$
$$= \int_V dV\,\psi_{n'=5,L'=2}R^2\psi_{n'=6,L'=0}. \tag{1.34}$$

For the radial part of the wave function ψ_{nL}, we can write [40]

$$R_{nL}(r) = -\left\{\left(\frac{2Z}{na_\mu}\right)^3\frac{(n-l-1)!}{2n[(n+l)!]^3}\right\}^{1/2}e^{-\rho(r)/2}\rho(r)^l L_{n-l-1}^{2l+1}(\rho(r)), \tag{1.35}$$

where $a_\nu = \frac{4\pi\epsilon_0\hbar^2}{\mu e^2} = a_0\frac{m_e}{\mu}$ is the reduced Bohr radius, $L_{n-l-1}^{2l+1}(\rho(r))$ are the associated Laguerre polynomials, and $\rho(r) = \frac{2Zr}{na_\nu}$. The valence electron of cesium sees an effective nuclear charge of $Z = 8.56$ [41]. When we use this in equation 1.35, we can calculate the reduced matrix element of equation 1.34. We then insert equation 1.34 and 1.33 in equation 1.32 to find a value $\langle n'F'||T^2||nF\rangle$. When we insert $\langle n'F'||T^2||nF\rangle$ into equation 1.31, we can calculate the individual saturation intensities of the hyperfine transitions of the quadrupole line. In table 1.3, we summarize the so-obtained saturation intensities. The results deviate from calculations in [9] where they did not discriminate between different $F \to F'$ levels.

1.2 Doppler-Free Spectroscopy

In vapor cells, various systematic effects play a role. Here, we discuss the effect of Doppler broadening. Due to the longitudinal Doppler effect, an atom with a velocity of $\boldsymbol{v} \ll c$ sees the frequency of incident light shifted by

$$\Delta\omega = \omega_{\mathrm{M}} - \omega_{\mathrm{R}} = -\boldsymbol{k} \cdot \boldsymbol{v}, \tag{1.36}$$

with the wavenumber $k = \frac{2\pi}{\lambda}$. ω_{M} and ω_{R} are the frequencies seen by a moving atom and by an atom in rest, respectively. An atom moving parallel to the laser beam with a velocity of $\boldsymbol{v}$ sees a laser frequency which is decreased by $\Delta\omega$ whereas for an atom moving antiparallel to the laser with a velocity of $\boldsymbol{v}$, the laser frequency is increased by $\Delta\omega$. Atoms will, therefore, absorb light with different frequencies depending on their velocity. The velocity distribution of an atomic ensemble is the source of so-called Doppler broadening of the spectrum. This broadening effect has the shape of a Gaussian distribution. The line profile of a Doppler-broadened spectral line is [42]

$$I(\nu) = I_0 \exp\left[-\left(\frac{c(\nu - \nu_0)}{\nu_0 v_{\mathrm{p}}} \right)^2 \right], \tag{1.37}$$

where ν_0 is the central frequency of an atomic emission line and $v_{\mathrm{p}} = (2k_{\mathrm{B}}T/m)^{1/2}$ is the most probable velocity with the atomic mass m, the temperature T, and the Boltzmann constant k_{B}. This Doppler profile has a full with at half maximum (FWHM) of

$$\delta\nu_{\mathrm{D}} = 2\sqrt{\ln 2}\frac{\nu_0 v_{\mathrm{p}}}{c} = \frac{\nu_0}{c}\sqrt{\frac{8k_{\mathrm{B}}T \ln 2}{m}}. \tag{1.38}$$

Using a frequency of $\nu = 437.602\,41$ THz, we find a Doppler width of $\delta\nu_{\mathrm{D}} = 465.49$ MHz for the $6S_{1/2} \to 5D_{5/2}$ transition at a temperature of $T = 293.15$ K. When we take the Lorentzian line shape that is associated with the natural linewidth of the atoms into account, the overall spectral profile corresponds to a Voigt distribution.

With narrow-band, tunable laser light sources, it is possible to overcome the limitations due to Doppler broadening. For this purpose, several techniques typically based on velocity selective absorption of atomic transitions have been developed. These techniques are summarized as nonlinear spectroscopy, because when optical pumping decreases the population density of the atoms in the ground state the absorbed radiation power depends nonlinearly on the incident power [43].

An example of Doppler-free laser spectroscopy is to use two polarized laser beams to induce birefringence in a vapor. This method is known as polarization spectroscopy [44]. Multiphoton spectroscopy can also be utilized to suppress Doppler broadening. For instance, in a two-photon transition, the Doppler shift is canceled when an atom is irradiated by two plane waves which travel in opposite directions [45].

However, the most common Doppler-free spectroscopy method is saturated absorption

spectroscopy, which is discussed in detail in the next section. For the measurements of this thesis, we use a modification of the usual saturated absorption spectroscopy method, because an emitter in a three-level configuration is investigated. The second part of the next section discusses this method.

1.2.1   Saturated Absorption Spectroscopy

With the Doppler-free spectrum obtained from saturation absorption spectroscopy and a frequency reference, it is possible to measure the absolute frequency of a transition of an atom. In principle, the precision to which we can determine these frequencies is limited only by the lifetime of the excited state.

The idea of saturated absorption spectroscopy is to send two counter-propagating laser beams, the pump beam and the probe beam, through an atomic vapor. The probe beam is used to measure the absorption spectrum of an optical transition with the resonance frequency ν_0, and the pump beam is used to deplete the ground state of this transition. The probe and the pump beam have the same frequency ν in the lab frame, but, since they are propagating in opposite directions, they feature opposite Doppler shifts in the atomic frame. If $\nu \neq \nu_0$, the pump beam will be absorbed by the velocity class $v_{x,pump} = (\nu - \nu_0)/k$ and the counter-propagating probe beam by the velocity class $v_{x,probe} = -(\nu - \nu_0)/k$. We will show an illustration of this in section 1.2.2. For $\nu \neq \nu_0$, the pump beam depletes a different velocity class than the velocity class which is probed by the probe laser. However, for $\nu = \nu_0$, we have $v_{x,pump} = v_{x,probe} = 0$ and the probe beam probes the velocity class which is depleted by the pump beam. Therefore, the probe laser will be less absorbed because there are fewer atoms in the ground state. Doppler-free lines will be visible as peaks in the transmission spectrum. These peaks correspond to dips in the absorption spectrum of the laser. These dips are commonly known as Lamb dips, because W.E. Lamb was the first to describe them theoretically [46].

Beside the Lamb dips, more peaks are possible in the saturated absorption spectrum. These peaks can occur when the pump and the probe beam are resonant with two separate transitions with resonant frequencies ν_1 and ν_2. Then the pump beam depletes the ground state via one transition, and the probe beam finds fewer atoms in the ground state and gets less absorbed on the second transition. This so-called crossover signals lie in the middle of two atomic resonances $\nu = \frac{\nu_1 + \nu_2}{2}$.

Figure 5 shows a possible realization of saturation spectroscopy. A laser is split up into a strong pump beam and a weak probe beam, which counter-propagate through a vapor cell. For many applications, it is not sufficient to send the beams crossed through the cell because the interaction region is very small and other solutions have to be found to maximize the beam overlap.

Typically, a photodiode can be used to measure the transmitted power of the probe beam. Alternatively, we can also measure the laser-induced fluorescence to get a
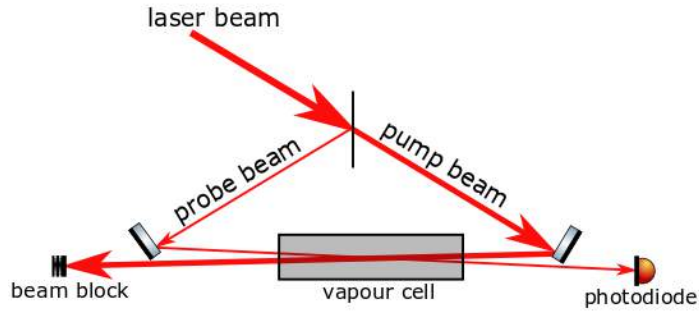
Figure 5: A possible realization of saturated absorption spectroscopy where a laser is split up into a strong pump beam and a weak probe beam. Both beams counter-propagate through a vapor cell, and a photodiode measures the intensity of the probe beam.

Doppler-free signal. In this kind of measurements, two counter-propagating beams from one laser are chopped at different frequencies and the modulation of the fluorescence is monitored at the sum frequency [47]. This technique has advantages when the absorption is small and the change of the attenuation of the probe beam is difficult to detect, because dips of the hyperfine lines can nearly disappear in the Doppler-broadened background [43].

In the setup explained in section 2.2, we use saturated absorption spectroscopy to stabilize the D2 laser at a wavelength of about $\lambda = 852\,\mathrm{nm}$ to a hyperfine transition of the D2 line of cesium. In section 2.3, this setup is extended to measure the hyperfine-resolved spectrum of the $6S_{1/2} \to 5D_{5/2}$ E2 transition. This extended setup is a modification of the typical saturated absorption spectroscopy setups, as explained in the next section.

1.2.2 Three-Level Spectroscopy with Two Lasers

In this thesis, we want to analyze the hyperfine structure of the $5D_{5/2}$ state of cesium experimentally. The ground state of cesium is the $6S_{1/2}$ state and it is possible to excite the atoms directly to the $5D_{5/2}$ state via an E2 transition. We can measure fluorescence of the decaying atoms between the $6P_{3/2}$ intermediate state and the $6S_{1/2}$ ground state. Typically, single-photon counting spectroscopy has to be used [48], because the fluorescence signal is very weak. This makes it difficult to apply the modulation and demodulation technique which we described in the last section.

Furthermore, the absorbed intensity of E2 transitions is very weak compared to the laser intensities which are necessary to saturate an E2 transition. Therefore, saturation spectroscopy as described in the previous section is very difficult to perform. We use another technique in this work to analyze the hyperfine structure of the $5D_{5/2}$ state. This technique is known as three-level Raman-type nonlinear spectroscopy [9, 12–14]. Figure 6 shows an illustration of this method. The basics are similar to typical satu-
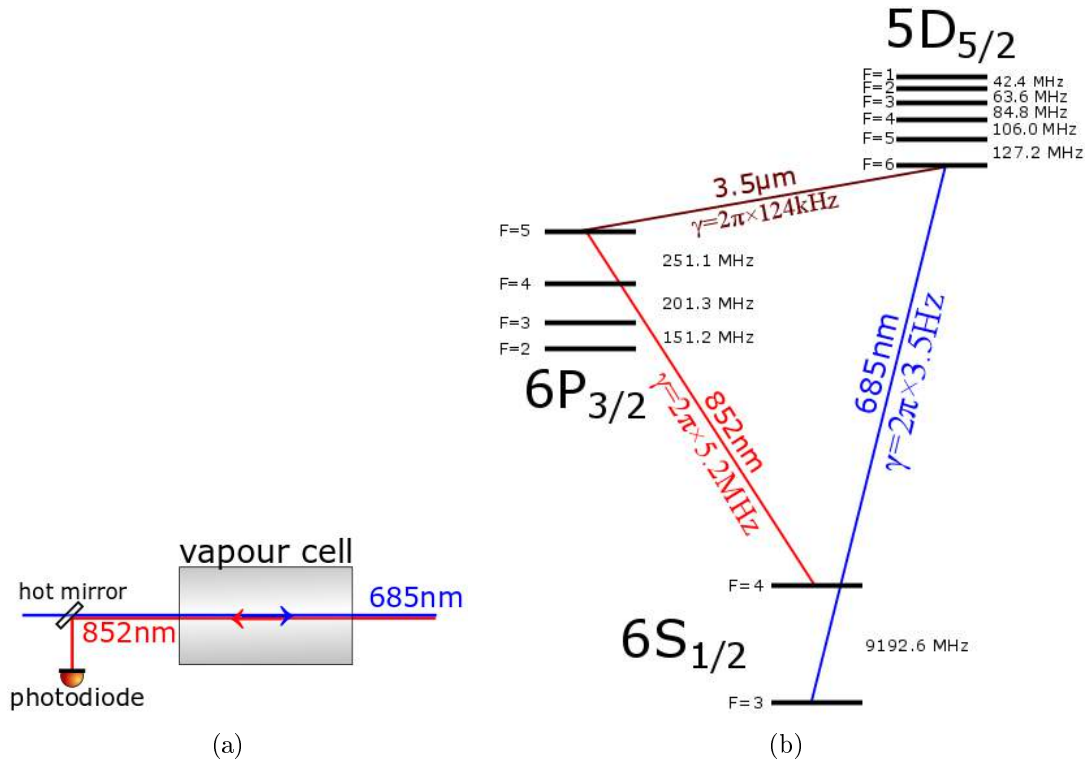
Figure 6: An illustration of three-level Raman-type nonlinear spectroscopy. (a) shows the spectroscopy setup. We will use the quadrupole laser at a wavelength of $\lambda = 685\,\mathrm{nm}$ as pump laser (blue) and the D2 laser at a wavelength of $\lambda = 852\,\mathrm{nm}$ as the probe laser (red). Both lasers share the same ground state. With a hot mirror, only reflecting near-infrared radiation, we separate the beams. A photodiode measures the probe beam after its transmission through a vapor cell. (b) shows one possible implementation that accounts for the atomic hyperfine structure. Here, atoms get "repumped" from the $6S_{1/2}(F = 3)$ level to the $6S_{1/2}(F = 4)$ level and therefore the probe laser gets more absorbed on resonance.

ration absorption spectroscopy. As before, a pump beam saturates a transition and a photodiode measures the transmitted power of a probe laser. However, now the lasers have different frequencies and address different transitions which only share the same ground state.

We use the quadrupole laser at a wavelength of $\lambda = 685\,\text{nm}$ as the pump laser. This laser excites atoms from the $6S_{1/2}$ to the $5D_{5/2}$ state. The D2 laser is the probe laser. This laser is stabilized to a hyperfine line of the $6S_{1/2} \leftrightarrow 6P_{3/2}$ transition and we measure its absorption. The intensity of the probe laser weak is in our case compared to the intensity of the pump laser, because of the higher saturation intensity of the quadrupole line. The probe laser always probes one velocity class of the atoms in the vapor cell while we scan the pump laser over all velocity classes. Regarding this, we show an illustration of the number of atoms in the ground state depending on the velocity class of atoms in figure 7. In contrast to two-level saturation spectroscopy, the pump beam and the probe beam do not have to counter-propagate through the vapor cell to obtain sub-Doppler resolution. This improved resolution can be achieved when the probe beam always probes one velocity class and is not scanned or when we lock the frequency of the probe laser on an independent reference.

When the pump laser excites atoms, the number density of atoms in the $6S_{1/2}$ state changes and therefore also the absorption of the probe beam changes. Considering the hyperfine structures of the states, shown in figure 6(b), a possible realization of the present saturation absorption spectroscopy is to lock the probe laser on the $6S_{1/2}(F = 4) \leftrightarrow 6P_{3/2}(F = 5)$ hyperfine transition and to scan the pump laser over the $6S_{1/2}(F = 4) \rightarrow 5D_{5/2}(F' = 2 - 6)$ transitions. The pump laser depletes the $6S_{1/2}(F = 4)$ level and, therefore, the probe laser gets less absorbed once the pump laser hits a resonance. We use a photodiode to record this change in the absorption of the probe laser as a function of the frequency of the pump laser.

We expect different results when we address the $6S_{1/2}(F = 3)$ level with the pump laser. When we scan the pump laser over the $6S_{1/2}(F = 3) \rightarrow 5D_{5/2}(F' = 1 - 5)$ transitions, the atoms get excited to the $5D_{5/2}$ state and then they will decay to the $6P_{3/2}$ state. From this state, the atoms can decay back to the $6S_{1/2}(F = 3)$ level, but they can also decay to the $6S_{1/2}(F = 4)$ state. This means that there will be more atoms in the $6S_{1/2}(F = 4)$ level and the quadrupole laser acts as a repumper from the $F = 3$ to the $F = 4$ level. When there are more atoms in the $6S_{1/2}(F = 4)$ level, we expect more absorption of the D2 laser when this laser still probes the $6S_{1/2}(F = 4) \leftrightarrow 6P_{3/2}(F = 5)$ transition.

The natural linewidth of the D2 transition is $\gamma_{6P6S} = 2\pi \times 5.223\,\text{MHz}$ [26]. This linewidth is one limitation of the maximum spectral resolution of the E2 transition resonances in our three-level spectroscopy technique [9]. However, as shown in [12,13,49], even in the ideal case disregarding experimental imperfections and constraints, it is not possible to achieve this resolution, because the second laser has another frequency.
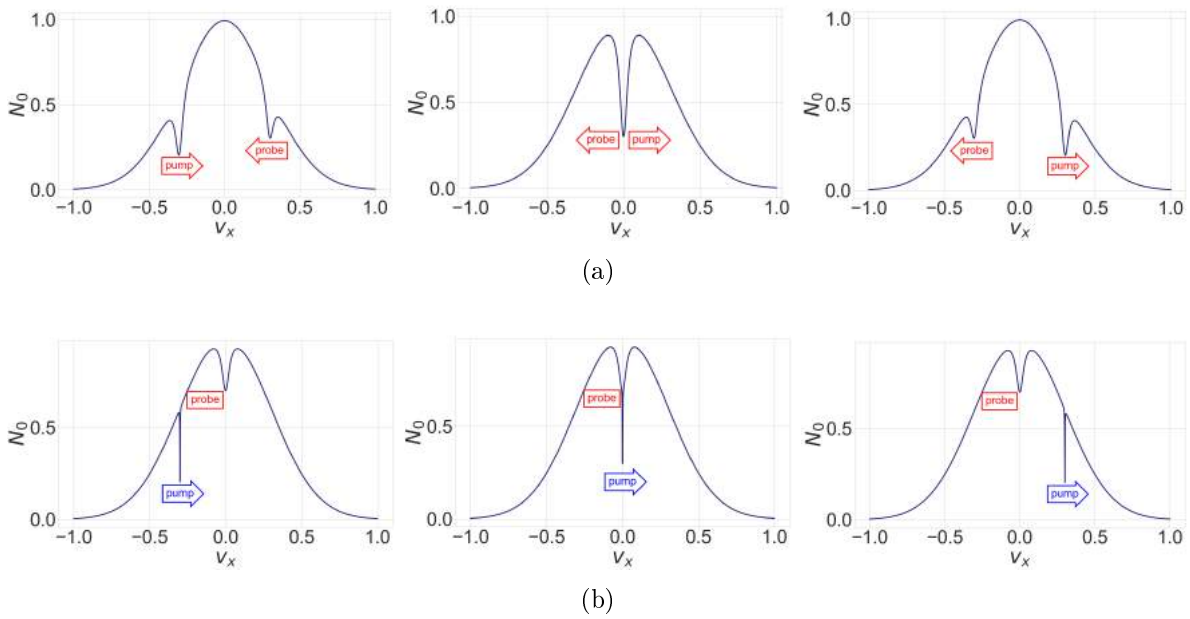
Figure 7: Illustrations of saturation absorption spectroscopy. In (a), two laser beams of the same frequency are simultaneously scanned. In (b), one laser has a fixed frequency, and the other one is scanned. N_0 is the number of atoms in the ground state and v_x is the velocity of the atoms in the propagation direction of the lasers. The arrows show the scanning direction of the laser beams and the boxes illustrate a frequency locked laser. In the illustrations on the left and the right, the laser beams address different velocity classes, and we do not see a Doppler-free spectrum. Only in the illustration in the center, when both beams address the same velocity class, we measure a modified absorption of the probe beam.

When we consider the frequency difference, the maximal spectral resolution is

$$\frac{\nu_{5D6S}}{\nu_{6P6S}} \times \gamma_{6P6S} = 2\pi \times 6.498 \, \text{MHz}, \tag{1.39}$$

where $\nu_{6P6S} = 351.721\,96 \, \text{THz}$ [26] and $\nu_{5D6S} = 437.598\,32 \, \text{THz}$ [27] are the frequencies of the D2 line and the quadrupole line, respectively. As a consequence, the resonance will always appear broader than what is expected from their natural linewidth. However, it is still sufficient to overcome the Doppler broadening and to resolve the hyperfine structure of the $5D_{5/2}$ state.

Chapter 2

Overview of the Experimental Setup

In this chapter, we present the setup and modifications which were necessary to perform the measurements presented in the following chapters. In the first section, we describe a setup which we use to detect fluorescence emitted from atoms which got excited via the $6S_{1/2} \to 5D_{5/2}$ E2 transition and then decay via the intermediate $6P_{3/2}$ state. In the second section, we discuss how we stabilize a laser at a wavelength of $\lambda = 852\,\mathrm{nm}$ to the D2 line of cesium. We use this laser in the last setup such that we can resolve the hyperfine structure of the $6S_{1/2} \to 5D_{5/2}$ E2 transition.

2.1 Fluorescence

In this section, we present a setup which we built to perform the fluorescence measurements of section 3.1. The setup is illustrated in figure 8. The idea is that the quadrupole laser excites atoms via the E2 transition from the $6S_{1/2}$ to the $5D_{5/2}$ state. Then, we use an SPCM to measure photons with a wavelength of $852\,\mathrm{nm}$ emitted when the atoms decay back to the ground state via the $6P_{3/2}$ intermediate state.

The quadrupole laser is a self-made external-cavity diode laser. For this laser at a wavelength of $\lambda = 685\,\mathrm{nm}$, we mounted a laser diode[1] in a housing which also contains a collimation tube with a collimation lens[2] to collimate the laser beam. We measure the temperature of the laser diode with a thermistor[3], and stabilize it with a Peltier element[4]. We use a controller[5] to regulate the temperature and the current which flows through the laser diode. With a home-built electronic circuit, we can modulate the laser frequency by modulating the current.

With an external cavity, we can select the operating wavelength of the laser diode and narrow the laser's optical spectrum. This cavity consists of a blazed grating[6] mounted in Littrow configuration. In this configuration, diffraction angle and incidence angle

---

[1]Thorlabs, HL6750MG
[2]Thorlabs, LT110P-B
[3]EPCOS/TDK, B57861S103F40
[4]Laird, PE-127-10-13
[5]Thorlabs, ITC102
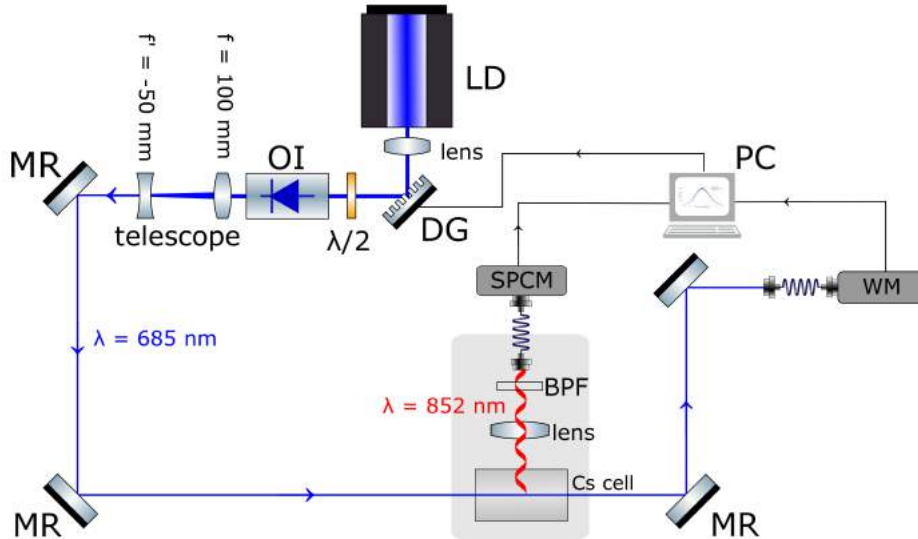[6]Thorlabs, GR13-1850

Figure 8: Setup for fluorescence spectroscopy. We excite atoms via the quadrupole line and record the fluorescence for the decay via the D2 line. (OI, optical isolator; BPF, bandpass filter; DG, diffraction grating; $\lambda/2$, half wave plate; MR, mirror; SPCM, single photon counting module; WM, wavelength meter).

are identical [42], and the frequency of the laser is changed by rotating the grating with a piezoelectric actuator.

After the laser beam leaves the laser housing, it passes a half wave-plate[7] which changes the polarization plane of the linearly polarized beam. We use an optical isolator to ensure that no reflected light from the setup reaches the laser. To align the optical isolator, we first mounted it in the wrong direction, and we adjusted the Faraday rotator for maximal extinction. Then, we turned the isolator around and mounted it, leaving the extinction ratio unchanged.

After the optical isolator, we inserted a telescope, because the beam diameter was too big for our requirements. After the laser beam passes the telescope, we use two mirrors to send it through a cesium vapor reference cell which has a length of 5.62 cm, a diameter of 2.4 cm, and contains 99.8 % cesium. In the cell, the cesium atoms are excited via the E2 transition between the $6S_{1/2}$ and the $5D_{5/2}$ state. The excited atoms decay mainly via the $6P_{3/2}$ state to the ground state by spontaneously emitting a photon at a wavelength of $\lambda = 3.5\,\mu\text{m}$ and a photon at a wavelength of $\lambda = 852\,\text{nm}$. We measure only the latter photons in the near-infrared, since we do not have any detectors for light at a wavelength of $\lambda = 3.5\,\mu\text{m}$. Because the fluorescence signal is very weak, we record it with an SPCM[8].

We use a lens with a focal length of $f = 50\,\text{mm}$ to collect fluorescence light. Following the lens, a bandpass filter[9] ensures that we measure only fluorescence photons and not scattered photons from the quadrupole laser beam. This also reduces the count rate

---

[7]Thorlabs, WPH05M-694
[8]Excelitas, SPCM-AQRH-14-FC
[9]Thorlabs, FBH850-10

due to room light that reaches the SPCM. We use a fiber holder which contains a lens to couple the fluorescence photons into a multimode fiber[10]. The fiber has a special cladding to make sure that no unwanted photons from, e.g., the room light are coupled into the fiber. Before we plugged this fiber into the SPCM, we connected a fiber check laser to the end of the fiber. This fiber check laser causes a radiation cone to exit at the other side of the fiber which allows one to determine the area from where fluorescence photons can be coupled into the fiber, i.e., the area from which we can detect fluorescence with the SPCM. With this method, we can pre-align the fiber, the fiber holder, the lens, the cesium cell, and the quadrupole laser beam in order to maximize the number of collected photons. Around these components, we built a box to block unwanted light and to protect the SPCM.

The SPCM generates a TTL pulse for every detected photon. We send these pulses with a BNC cable to a shielded connector block[11], which we connect to a computer via a PCI-card[12]. A LabVIEW program counts the total number of pulses measured within a certain time. This program can also detect the frequency of the quadrupole laser beam when we measure it with a wavelength meter[13].

2.2   Locking a Laser to the D2 Line of Cesium

In the first part of this section, we present the setup which we used to stabilize the D2 laser to the D2 line of cesium. In the second part, we discuss measurements of the absorption spectrum with the Lamb peaks of the D2 line.

2.2.1   Setup of the Lock

We use a three-level Raman-type nonlinear spectroscopy method to measure the hyperfine structure of the $6S_{1/2} \rightarrow 5D_{5/2}$ E2 transition of cesium by measuring the modified absorption of the $6S_{1/2} \rightarrow 6P_{3/2}$ transition. For this task, we have to lock a probe laser to one of the hyperfine transitions of the D2 line. In this section, we present the setup that allows us to lock this laser, see figure 9.

We built the D2 laser at a wavelength of about $\lambda = 852\,\mathrm{nm}$, similar to the external cavity laser from the last section. We mounted a laser diode[14] in a collimation tube, and we use a diffraction grating[15] to form the cavity. A controller[16] regulates the temperature and current of the laser diode. The frequency of the laser changes when we alter the angle of the grating with a piezo. We use a function generator[17] to apply a

---

[10]Thorlabs, FG050LGA
[11]National Instruments, BNC-2110
[12]National Instruments, PCI-6221
[13]HighFinesse, WS-6, Serial No. 706
[14]Roithner Lasertechnik, RLT850-100GS
[15]Thorlabs, GR13-1205
[16]Arroyo Instruments, 6305 ComboSource, 500mA
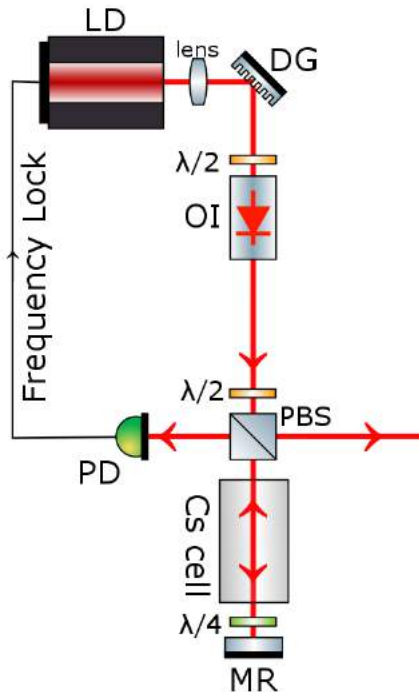[17]Voltcraft, FG-7202

Figure 9: An illustration of the setup which we use for the frequency stabilization of the D2 laser. (OI, optical isolator; DG, diffraction grating; $\lambda/2$, half wave plate; $\lambda/4$, quarter half plate; MR, mirror; PBS, polarizing beam splitter; PD, photodiode).

voltage to the piezoelectric actuator to scan the frequency of the laser periodically. Following the grating, an optical isolator prevents unwanted feedback into the optical diode. We then mount a half-wave plate and a polarizing beam splitter[18] in the beam path. This allows us to control the power that is sent to the frequency lock and the main fluorescence setup. We use the transmitted beam for a Doppler-free saturated absorption spectroscopy setup which enables us to resolve the hyperfine spectrum of the $6S_{1/2} \rightarrow 6P_{3/2}$ transition. We explained this spectroscopy method in detail in section 1.2.1. In the present implementation, the laser beam transmits through a cesium cell[19] with a length of 5 cm and a diameter of 2.62 cm. After the beam passes the cell, it is reflected by a mirror and passes the cell in the other direction a second time. In between the cell and the mirror, we mounted a quarter-wave plate[20]. The beam polarization is rotated by 180° because the beam passes this plate two times. Therefore the transmitted beam gets now reflected by the polarizing beam splitter and can be measured. We detect the power of the beam with a photodiode[21] and see an absorption spectrum with the peaks associated with the hyperfine levels of the $6P_{3/2}$ state.

We use a frequency modulation and demodulation technique for stabilization of the frequency of the D2 laser. In figure 10, we illustrate how we implement this method

---

[18] Thorlabs, PBS122
[19] Thorlabs, Cs S128
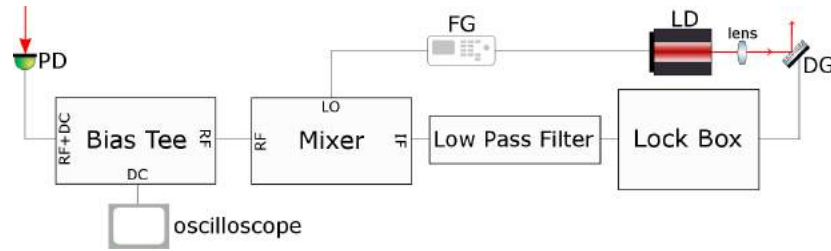[20] Thorlabs, WPQ05M-850
[21] Farnell, BP104S-Z

Figure 10: The components which are used to stabilize the frequency of the laser to the D2 line of cesium. We use a photodiode to measure the power of the laser beam. Depending on this signal, the angle of the diffraction grating is changed so that the frequency of the laser stays the same (DC, direct current signal; DG, diffraction grating; FG, frequency generator; IF, intermediate frequency; LD, laser diode; LO, local oscillator; PD, photodiode; RF, radio frequency signal).

into our setup. To describe it, let us consider a signal $S(\nu)$ that depends on the laser frequency ν. When performing amplitude modulation, this signal is transformed to $S_{AM}(t, \nu) = \cos^2(\omega t) S(\nu)$. Demodulating the resulting signal at ν yields the initial signal S. When performing FM, the initial signal transforms to

$$S_{FM}(\nu, t) = S(\nu + \epsilon \cos(\omega t)) = S(\nu) + \epsilon \cos(\omega t) \frac{\mathrm{d}S(\nu)}{\mathrm{d}\nu} + \mathcal{O}(\epsilon^2). \tag{2.1}$$

The demodulation yields a signal that is, to first order, proportional to the derivative of the initial signal. We use FM because a laser lock works better with the steeper slope of the derivative of the initial signal. Furthermore, we lock the laser on the zero crossing of the derivative which makes the lock more resistant against power fluctuations of the laser. We use an electronic circuit, connected between the controller and the laser diode, to modulate the current which flows through the laser diode. A frequency generator[22] periodically modulates this current and, therefore, the laser beam gets frequency modulated accordingly.

The beam power is recorded using a photodiode that is fast enough to measure the modulation frequency. We connect the photodiode to the RF+DC input of a bias tee[23], which separates the modulated RF signal from the DC signal. With an oscilloscope, we can display the DC signal which looks similar to the signal in figure 11(a). We send the radio frequency signal to the RF input of a frequency mixer[24]. We connect the frequency generator which we use for the laser modulation to the LO input of the mixer. When we apply a signal with the right phase and the same frequency as the modulation frequency, the signal from the photodiode gets demodulated. A low pass filter[25], connected to the IF output of the mixer, suppresses signals with high frequencies. After this filter, we send the demodulated signal to a homemade

---

[22]Rigol, DG1022
[23]Mini Circuits, ZFBT-4R2GW+
[24]Mini Circuits, ZX05-1MHW-S+
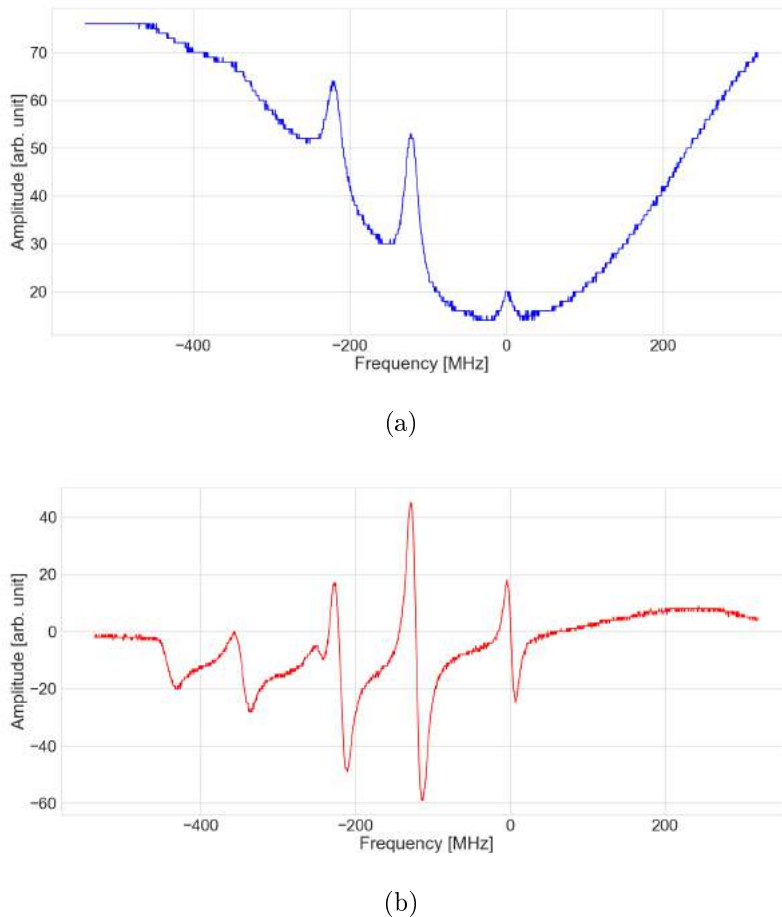[25]Mini Circuits, SLP-1.9+

(a)

(b)

Figure 11: Hyperfine-resolved spectra of the D2 line when we scan the frequency around the $6S_{1/2}(F = 4) \rightarrow 6P_{3/2}(F' = 3 - 5)$ states. (a) The signal from the DC output of the bias tee. (b) The demodulated signal at the monitor connector of the lockbox. A sinus with a frequency of $5\,\mathrm{MHz}$ and a peak-to-peak amplitude of $100\,\mathrm{mV}$ was used for the modulation. For the demodulation, we applied a sinus with a frequency of $5\,\mathrm{MHz}$ and an amplitude of $100\,\mathrm{mV}$ to the mixer. At the mixer, the two signals have a phase difference of about $\Delta\phi \approx 0$. We used the crossover peaks $F = 3/5$ and $F = 4/5$, and literature values [50] to convert the measured time axis into a frequency axis. We can see that the demodulated signal is the derivative of the initially measured voltage.

PI-lockbox[26]. This lockbox controls the piezo behind the diffraction grating of the laser. The monitor connector of the lockbox outputs the demodulated signal, shown in figure 11(b). We then change the scanned frequency range to investigate only one hyperfine peak and lock the laser on the zero crossing of the derivative of this peak.
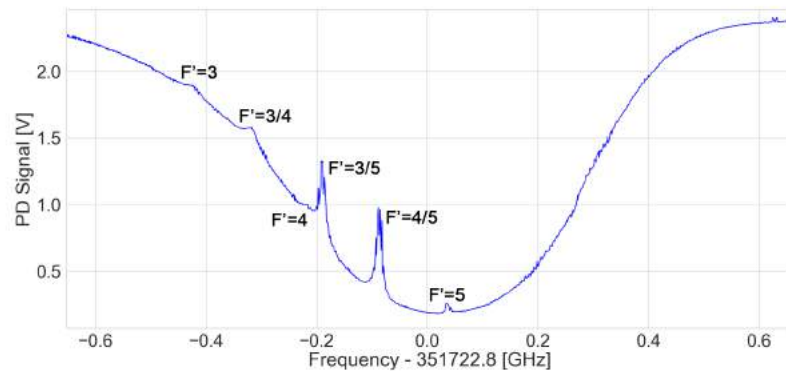
2.2.2   Measurements of the D2 Line

In this section, we present measurements of a saturated absorption spectrum of the D2 line of cesium featuring Lamb peaks. By using a triangle function of a waveform

---

[26]Lockbox Vers.5
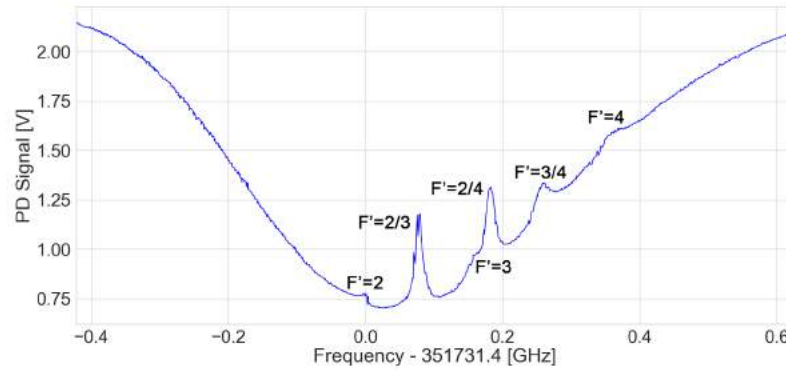
(a)

(b)

Figure 12: Measured transmission spectra featuring dips of the hyperfine levels of the D2 line. In (a), we scanned the laser over the $6S_{1/2}(F = 3) \rightarrow 6P_{3/2}$ transition. In (b), we scanned the laser over the $6S_{1/2}(F = 4) \rightarrow 6P_{3/2}$ transition. We labeled the hyperfine levels of the $6P_{3/2}$ state in the spectrum. In the middle of every pair of hyperfine levels are crossover peaks, labeled with the two numbers of the corresponding hyperfine levels.

generator to scan the frequency of the laser, we were able to take the measurements shown in figure 12. For this purpose, a LabView program was used which enables us to detect the voltage of the photodiode and the frequency of the wavelength meter simultaneously. Because of timing issues, we used a relatively low scanning frequency of about 100 mHz. We averaged over six scanning cycles to increase the signal-to-noise ratio. By using a current of 93.0 mA and a temperature of 30 °C to operate the D2 laser diode, we were able to scan over the $6S_{1/2}(F = 4) \rightarrow 6P_{3/2}$ transition completely. We present the transmission spectrum with the hyperfine peaks in figure 12(a). To scan over the $6S_{1/2}(F = 4)$ level, we used a current of 99.4 mA and a temperature of 30 °C to run the D2 laser diode. Figure 12(b) shows this spectrum.

The saturation absorption spectroscopy measurements of the D2 line give results which are compatible with measurements of other groups [51]. Furthermore, they are in good agreement with the level scheme from section 1.1.4. In table 2.1, the frequencies of the D2 hyperfine-resolved transitions are shown and compared to literature values

Table 2.1: Absolute frequency measurements of the hyperfine transitions of the D2 line. The quantum number F and F' correspond to the hyperfine levels of the $6S_{1/2}$ state and the $6P_{3/2}$ state, respectively. For the measured frequencies of this thesis, the error limits are estimated to 10 MHz. The literature values were taken from [50].

| | F=3 Frequency - 351.73 THz [GHz] | | F=4 Frequency - 351.72 THz [GHz] | |
	this work	literature	this work	literature
F'=2	1.40	0.55		
F'=3	1.56	0.70	2.38	1.51
F'=4	1.76	0.90	2.58	1.71
F'=5			2.77	1.96

from [50]. The frequency spacing between the measured lines agree excellently with the literature values, but we see a shift of the absolute frequency. This shift of in average 0.85 GHz probably results from insufficient and outdated calibration of the wavelength meter.

2.3   Spectroscopy of the $5D_{5/2}$ Hyperfine States

In this section, we present the setup which is illustrated in figure 13. This is a three-level Raman-type nonlinear spectroscopy setup which we use to resolve the hyperfine spectrum of the $6S_{1/2} \rightarrow 5D_{5/2}$ E2 transition. Furthermore, we are able to stabilize the quadrupole laser to one of the hyperfine transitions of the quadrupole line.

We use the saturation absorption spectroscopy setup, as presented in the last section, to lock the D2 laser to a specific $F \rightarrow F'$ transition of the D2 line. This laser is the probe laser in the present setup whereas the quadrupole laser acts as the pump laser. We split the probe laser with a polarizing beam splitter and use the transmitted component for the locking of this laser. The other component is reflected towards the rest of the setup. We use a combination of a have wave plate, a polarizing beam splitter, and a beam block to adjust the power of the beam.

With the probe laser beam set to the desired intensity, we combine it with the pump laser using a hot mirror[27]. The two laser beams propagate in opposite directions through a 5 cm long cesium vapor cell[28]. Then, we separate the probe laser from the pump laser with another hot mirror. After separating the beams, we measure the power of the probe laser with a photodiode[29]. A bandpass filter[30] with a central wavelength of 850 nm and a FWHM of 10 nm in front of the photodiode improves the extinction of scattered light especially from the pump laser.

The beam path of the pump laser is similar to that of the quadrupole laser in section 2.1. We only extended it by the cesium cell where the pump laser is counter-propagating

---

[27]Thorlabs, M254H45
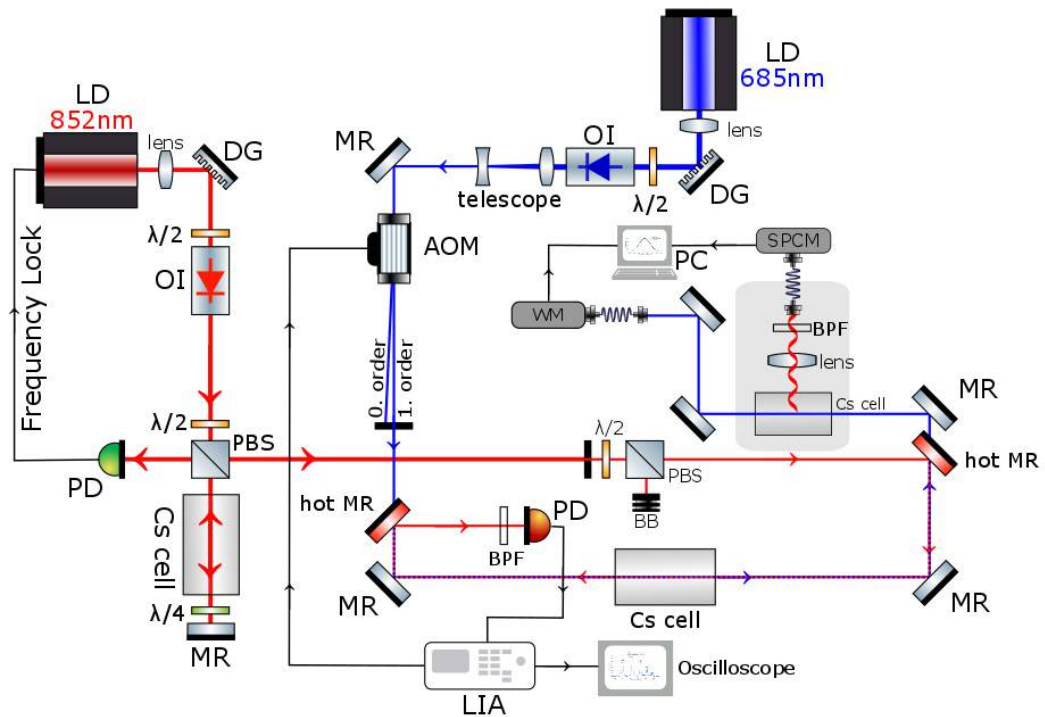[28]Thorlabs, Cs S132
[29]rev4_01
[30]Thorlabs, FBH850-10

Figure 13: Setup for hyperfine-resolved spectroscopy of the $6S_{1/2} \to 5D_{5/2}$ E2 transition (AOM, acousto-optic modulator; BB, beam block; OI, optical isolator; BPF, bandpass filter; DG, diffraction grating; $\lambda/2$, half wave plate; $\lambda/4$, quarter half plate; LIA, lock-in amplifier; MR, mirror; PBS, polarizing beam splitter; PD, photodiode; SPCM, single photon counting module; WM, wavelength meter).

with the probe laser. The pump laser depletes the ground state of cesium, and this changes the absorption of the probe laser which we measure with the photodiode. Because the changes of the absorption are small, it was necessary to use a modulation technique in order to improve the signal-to-noise ratio. In the present setup, an AOM[31] diffracts the pump laser into several orders. We select the minus first order with an aperture and send it through the cesium cell whereas the other beams are blocked. A waveform generator[32] and an amplifier[33] provide the 110 MHz RF signal to drive the AOM. The waveform generator allows us to amplitude or frequency modulate the output signal and, thus, allows us to modulate the diffracted orders of the AOM. The modulation frequency is provided by a lock-in amplifier[34] which also demodulates the measured power of the probe laser. Because we use the same frequency for the modulation and the demodulation, only modulated signals of the probe laser are visible after the demodulation. We modulate only the pump laser, therefore exclusively signals of the probe laser which are caused by the pump laser are visible when the signal is demodulated.

We measure the demodulated signal of the lock-in amplifier with an oscilloscope[35] or we can use this signal to lock the pump laser. When we want to stabilize this quadrupole laser, we use FM, since this yields a signal proportional to the derivative of the initial signal. We send the demodulated signal of the probe laser to a home-built PI-lockbox. We also connect the second channel of the waveform generator to this lockbox. This channel provides the scanning frequency of the diffraction grating. Similar to the setup in section 2.2, a switch can be operated, and the lockbox changes the voltage of the piezo automatically. This changes the angle of the diffraction grating of the quadrupole laser so that the frequency of the laser is stabilized.

---

[31] AA Opto Electronic, MT110-B50A1-VIS
[32] RIGOL Technologies, DG4162
[33] Mini Circuits, ZHL-1-2WX(+)
[34] Stanford Research Systems, SR830
[35] Teledyne LeCroy, HDO4054

Chapter 3

Spectroscopy of the $5D_{5/2}$ Hyperfine States

In this chapter, we present hyperfine-resolved spectra of the cesium $6S_{1/2} \rightarrow 5D_{5/2}$ E2 transition. In the first section, we discuss measurements of fluorescence emitted upon excitation of the atoms to the $5D_{5/2}$ state and decay via the intermediate $6P_{3/2}$ state back to the ground state. Then, we perform three-level Raman-type nonlinear spectroscopy and use different configurations of the probe and the pump laser to resolve the hyperfine structure of the quadrupole line. We experimentally investigate the dependence on the power of the pump laser and the probe laser, and the role of the pump laser AM frequency. In the last part of this chapter, we discuss how to stabilize a laser to the quadrupole line.

3.1 Fluorescence Related to the $6S_{1/2} \rightarrow 5D_{5/2}$ Transition

In the first measurement of this chapter, we investigate the fluorescence signals emitted upon excitation of the atoms on the $6S_{1/2} \rightarrow 5D_{5/2}$ E2 transition. Similar experiments were performed in [9]. We use the quadrupole laser to excite the atoms to the $5D_{5/2}$ state from where they will decay mainly to the $6P_{3/2}$ state and then back to the $6S_{1/2}$ ground state by emitting a photon at a wavelength of $\lambda = 3.5\,\mu m$ and a consecutive photon at a wavelength of $\lambda = 852\,nm$. In figure 14, we detect the $852\,nm$ photons with an SPCM.

For this measurement, we used a copper wire at a temperature of $103\,°C$ to heat the cell in order to increase the cesium pressure. This increases the fluorescence signal by a factor of about 17 compared to a cell at room temperature. The laser power was $33.2\,mW$ in front of the cell, and we continuously scanned the laser frequency with a triangle function with a frequency of $10\,mHz$ across the atomic resonance. We use a LabView program to count the detected photons in a time span of $20\,ms$. At the same time, we record the frequency of the quadrupole laser with a wavelength meter thereby
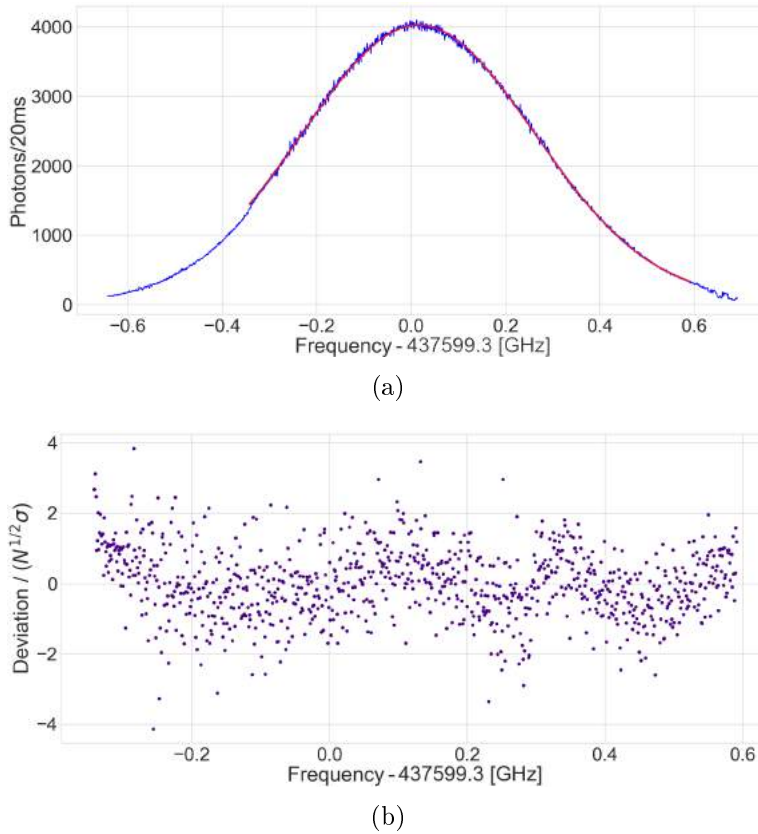
(a)

(b)

Figure 14: Fluorescence excitation spectrum at a wavelength of around $\lambda = 852\,\mathrm{nm}$ when only the quadrupole laser is present and its frequency is being scanned. (a) We fitted the measurement (blue) with a Gaussian function (red). Because of laser instabilities due to mode hopping, we only fit the frequency interval between $437\,598.96\,\mathrm{GHz}$ and $437\,599.89\,\mathrm{GHz}$. (b) When we calculate the residuals, we see a deviation between the measured Doppler-broadened fluorescence and the Gaussian fit which is a sign for a finer structure of the quadrupole line.

measuring the absolute frequency of the fluorescence light.

We scanned the frequency of the quadrupole laser around the $6S_{1/2}(F = 4) \rightarrow 5D_{5/2}(F' = 1-6)$ transitions. From the E2 selection rules, we know that we can excite the atoms to the $F' = 2-6$ levels. In the present case, we did not use a Doppler-free technique, and the signals are broadened. Therefore, the hyperfine levels of the $5D_{5/2}$ state cannot be resolved. The reason being is that there is a is the small frequency splitting between the hyperfine lines compared to Doppler broadening at room temperatures of about $500\,\mathrm{MHz}$ given by equation 1.38.

The Doppler broadening leads to a Gaussian profile. Therefore, we use a Gaussian function to fit our measurement as presented in figure 14(a). Due to laser instabilities, we did not fit the whole spectrum. To analyze the quality of the fit, we calculate the residuals. In figure 14(b), we divide the residuals by $\sqrt{N}\sigma$, where N is the number of measured photons in a time interval of $20\,\mathrm{ms}$ and σ is the standard deviation of the residuals. We observe that the residuals are distributed asymmetrically. From this, we conclude that several lines contribute to the signal [9].

We, therefore, superimpose five Gaussian functions in order to account for the five transitions expected from the E2 selection rules. We fix the relative weights, calculated with equation 1.19, and the relative frequencies of the hyperfine levels for the fit. Our free fit parameters are thus a global amplitude, a global frequency shift, a global FWHM, and a global offset. We find an improved fit compared to the fit with only one Gaussian as shown in figure 15. In figure 15(a), we present the fit and the five superimposed Gaussian profiles. Figure 15(b) shows the residuals of the fit. Except for small deviations which occur probably because of laser instabilities, these residuals indicate an improved fit. From the fit, we find that the FWHM of the Gaussians is $506(34)\,\mathrm{MHz}$ which is in agreement with our calculations of Doppler broadening in section 1.2.

3.2 Measurement of the $5D_{5/2}$ Hyperfine States

We now use three-level Raman-type nonlinear spectroscopy to measure hyperfine-resolved spectra of the $6S_{1/2} \rightarrow 5D_{5/2}$ E2 transition. We use a probe laser, stabilized to the D2 line as explained in section 2.2, and scan a pump laser across the quadrupole line. First, we scan the pump laser around the $6S_{1/2}(F = 4) \rightarrow 5D_{5/2}(F' = 2-6)$ transitions, and then we scan around the $6S_{1/2}(F = 3) \rightarrow 5D_{5/2}(F' = 1-5)$ transitions. This results in different hyperfine-resolved spectra of the quadrupole line as discussed in the following sections.
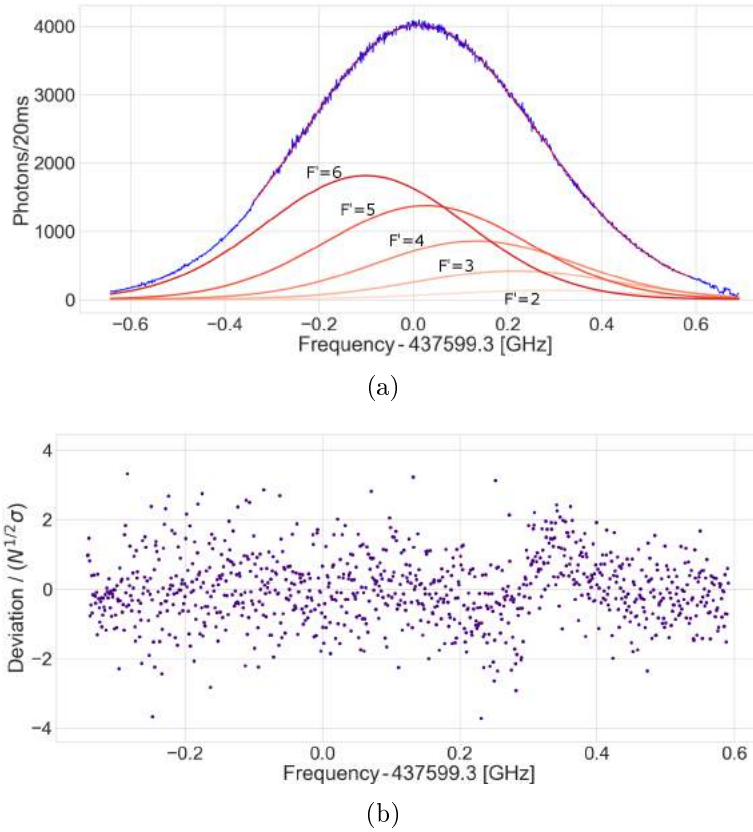
(a)

(b)

Figure 15: Fit of the fluorescence excitation spectrum. (a) As fit function, we superimposed five Gauss functions, labelled with the addressed hyperfine levels of the $5D_{5/2}$ state. We fit the same frequency interval as in figure 14. (b) We see that the distribution of the residuals has improved compared to a fit with only one Gaussian profile. The deviations on the right side occur probably because of laser instabilities.
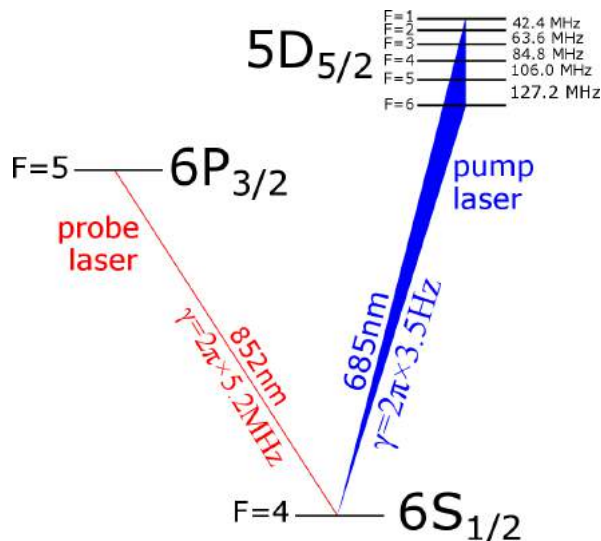
Figure 16: Depletion of the $6S_{1/2}(F = 4)$ level. We present the relevant hyperfine levels which are addressed by the probe laser and the pump laser. To measure a hyperfine-resolved spectrum of the $6S_{1/2}(F = 4) \rightarrow 5D_{5/2}$ E2 transition, the probe laser is stabilized to the D2 line while the pump laser is scanned over the quadrupole line. Both lasers excite the atoms from the $6S_{1/2}(F = 4)$ level.

3.2.1 Depletion of the $6S_{1/2}(F = 4)$ State

Here, we study the hyperfine-resolved spectrum of the $6S_{1/2}(F = 4) \rightarrow 5D_{5/2}(F' = 2 - 6)$ E2 transition via depletion of the $6S_{1/2}(F = 4)$ state. In figure 16, we illustrate which states are addressed by the pump and probe laser. The pump laser depletes the $6S_{1/2}(F = 4)$ level; thus, the number density of atoms in this level is reduced. As a consequence, the absorption of the probe laser, stabilized to the $6S_{1/2}(F = 4) \rightarrow 6P_{3/2}(F' = 5)$ transition, is reduced. In order to measure this effect, we detect the power of the probe laser transmitted through the cesium cell with a photodiode. Less absorption of the probe laser corresponds to peaks in the transmission spectrum as shown in figure 17. Because of the discussion in section 1.2.2, we see a Doppler-free spectrum of the $6S_{1/2} \rightarrow 5D_{5/2}$ E2 transition.

For this measurement, the pump laser had a beam waist of approximately $0.2\,\mathrm{mm}$. Without amplitude modulation, the power was about $20.5\,\mathrm{mW}$ in front of the cell corresponding to a peak intensity of $I_0 = 15.6\,\mathrm{W/cm^2}$. When we compare this value to the saturation intensities of the hyperfine transitions of the quadrupole line, shown in table 1.3, we find that it should be large enough to saturate all transitions. The intensity of the probe laser was about $I_0 = 55\,\mathrm{mW/cm^2} \approx 20.3 I_{\mathrm{sat}}$. This intensity is relatively high in order to transmit enough power through the vapor cell to reach the photodiode and to get a measurable signal. To scan the frequency of the pump laser, we applied a triangle function with a frequency of $4\,\mathrm{Hz}$ and a peak-to-peak amplitude of $200\,\mathrm{mV}$ to the piezoelectric actuator of the diffraction grating. We use an AOM to amplitude modulate the pump laser beam with a frequency of $15\,\mathrm{kHz}$. This frequency
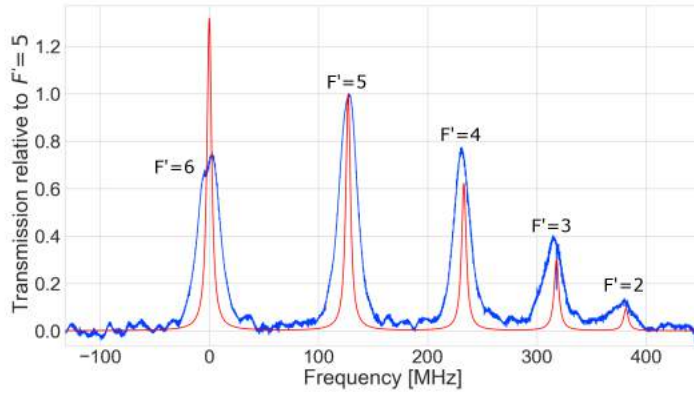
Figure 17: Doppler-free spectrum of the quadrupole line. We labeled the lines with the addressed hyperfine levels of the $5D_{5/2}$ state. We stabilized the probe laser to the $6S_{1/2}(F = 4) \rightarrow 6P_{3/2}(F' = 5)$ transition and scanned the frequency of the pump laser over the $6S_{1/2}(F = 4) \rightarrow 5D_{5/2}$ E2 transition. The measurement (blue) is compared to theoretical calculations (red). The experimental spectrum is an average of ten spectra. The frequency is shown relative to the frequency to the $F' = 6$ line and the measured power of the transmission relative to the $F' = 5$ line. We clearly resolve the transmission peaks corresponding to the $F' = 2 - 6$ levels of the $5D_{5/2}$ state.

Table 3.1: Settings of the Lock-in amplifier used to modulate the pump beam and to demodulate the measured intensity of the probe beam.

Input	A	Sensitivity	2x1 mV
Couple	AC	Phase	+150 DEG
Ground	Ground	Ampl	2.5 V
Time constant	1x100 μs	Mod. Freq	15 kHz
Slope	24 dB	Source	Internal

is provided by a Lock-in amplifier which also demodulates the detected signal. Table 3.1 shows the settings of the Lock-in amplifier.

We measure the voltage of the demodulated signal of the photodiode over time and use the $F' = 6$ line and the $F' = 5$ line for the calibration of the frequency axis. The spectrum, depicted in figure 17, is an average of ten individually detected spectra.

The pump laser excites the atoms from the $6S_{1/2}$ state via an E2 transition to the $5D_{5/2}$ state. The quadrupole selection rules determine to which hyperfine states transitions are possible. These selection rules state that $\Delta F = 0, \pm 1, \pm 2$. Because the atoms are excited from the $6S_{1/2}(F = 4)$ level, we can see the $F' = 2 - 6$ levels of the $5D_{5/2}$ state in the spectrum.

The line intensities depend on the population of the $6S_{1/2}(F = 4)$ level. The number density of atoms in this level gets lower when atoms are excited to the $5D_{5/2}$ state by the pump laser. The excited atoms can decay via the $6P_{3/2}$ state back to the $6S_{1/2}(F = 4)$ level, thereby increasing the number density of atoms in this level again. We use equations 1.18 and 1.19, which describe the line strength of an E1 and an E2 transition, to calculate the expected line intensities in case of a Doppler-free hyperfine-resolved

spectrum. The signal strength is given by [9]

$$S(F') = S_{F,F'}^{Q} - \alpha \sum_{F''} S_{F,F'}^{Q} S^{D}(F', F'') S^{D}(F'', F), \tag{3.1}$$

where F, F' and F'' are the toal quantum numbers of the hyperfine levels of the $6S_{1/2}$, $5D_{5/2}$ and $6P_{3/2}$ state, respectively. The sum runs over all hyperfine levels F'' of the $6P_{3/2}$ state. The re-pumping ratio α is given by [9]

$$\alpha = \frac{\gamma_{5D6S} + \gamma_{5D6P}}{\gamma_{\rm t} + \gamma_{5D6S} + \gamma_{5D6P}}, \tag{3.2}$$

where γ_{5D6S} and γ_{5D6P} are the partial decay rates from the $5D_{5/2}$ state to the $6S_{1/2}$ state and the $6P_{3/2}$ state, respectively. γ_t describes a transit relaxation which diminishes the re-pumping back to the ground state mainly because of the relative long lifetime of the $5D_{5/2}$ state. This rate can be approximated by [9]

$$\gamma_{\rm t} \approx \frac{2v_{\rm t}}{d} \approx 848.64\,{\rm kHz}, \tag{3.3}$$

where $d \approx 400\,\mu{\rm m}$ is the beam diameter in the middle of the cell and

$$v_{\rm t} = \int\limits_{-\infty}^{+\infty} {\rm d}v_x \int\limits_{-\infty}^{+\infty} {\rm d}v_y \int\limits_{-\infty}^{+\infty} {\rm d}v_z \sqrt{v_x^2 + v_y^2} \left(\frac{m}{2\pi {\rm k_B} T} \right)^{3/2} \exp\left[-\frac{m\boldsymbol{v}^2}{2{\rm k_B} T} \right]$$
$$= \frac{1}{2}\sqrt{\frac{2\pi k_{\rm b} T}{m}} = 169.727\,{\rm m/s}, \tag{3.4}$$

is the transverse mean thermal velocity across the laser beam for a temperature of $T = 293.15\,{\rm K}$. We find a ratio of $\alpha = 0.48$, which we use to calculate the expected relative strengths of the experimentally observed lines.

In figure 17, we superimpose five Lorentz functions, one for every hyperfine line of the $5D_{5/2}$ state, to find the expected hyperfine-resolved spectrum. We used equation 3.1 to calculate the relative strenghts of the functions, and equation 1.39 determines their FWHM. We observe that the hyperfine structure of the $5D_{5/2}$ state is resolved and the lines have the expected relative frequencies. The relative line intensities coincide with our calculations except for the $F' = 6$ line. We discuss these deviations in detail in section 3.3.3. The measured linewidths are broader than expected. This broadening could be a consequence of power broadening, transit time broadening, pressure broadening, and laser frequency jitter. The transit time broadening is negligible, since it can be calculated as [42]

$$\delta\nu \approx 0.4\frac{v_{\rm t}}{w} \approx 340\,{\rm kHz}, \tag{3.5}$$

with $w \approx 200\,\mu{\rm m}$ corresponding to the beam waist of a Gaussian beam profile. This is small compared to the other broadening effects. We probably have some pressure
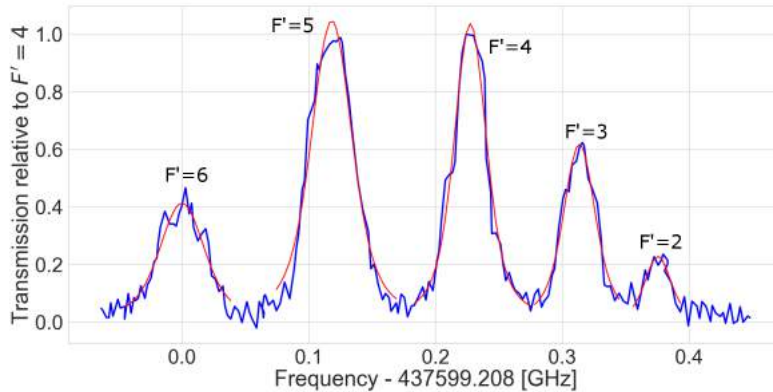
Figure 18: Absolute frequency measurement (blue) of the quadrupole line. We used a wavelength meter to record the frequency of the hyperfine-resolved spectrum of the $6S_{1/2}(F = 4) \rightarrow 5D_{5/2}$ E2 transition. We fitted Voigt profiles (red) to the experimental data to find the absolute frequencies presented in table 3.2.

Table 3.2: The absolute frequency values of the transitions between the $6S_{1/2}(F = 4)$ level and the hyperfine levels of the $5D_{5/2}$ state measured with a wavelength meter. The error corresponds only to the error of the fit. We compare our measured line intensities to literature values of relative frequencies [25] since we did not find an absolute frequency measurement.

	Our measured line frequency - 437 599.208 GHz [MHz]	Literature values of the relative frequencies [MHz] [25]
F=6	0 ± 0.8	0
F=5	118.1 ± 0.4	127.2
F=4	227.5 ± 0.4	233.2
F=3	313.6 ± 0.5	318
F=2	375.5 ± 0.8	381.6

broadening, but this effect should be negligible at room temperature for our error bars [23]. A possible broadening of the lines can arise from the quadrupole laser frequency jitter which we cannot estimate. However, the best candidate to explain the broadening of the lines in the experimental spectrum is power broadening due to the probe laser. We will discuss this in section 3.3.2. In the end, the natural linewidth of the D2 line limits the FWHM of the lines. A possible solution to get even narrow lines could be to probe another transition, for example, the $6S_{1/2} \rightarrow 7P_{1/2}$ E1 transition of cesium. We will discuss this point in the outlook.

In figure 18, an absolute frequency measurement is shown. We used a LabView program to read out a PCI-card and the measured frequency of the wavelength meter. This allows us to record the demodulated transmission signal of the probe laser and the frequency of the pump laser simultaneously. The pump laser was amplitude-modulated with a frequency of 30 kHz and scanned with a triangle function with a frequency of 20 mHz over the $6S_{1/2}(F = 4) \rightarrow 5D_{5/2}$ E2 transition.

The frequency resolution of this measurement is worse compared to the other measure-

ments. However, we can fit a Voigt profile to the lines to find the absolute frequencies shown in table 3.2. We did not take systematic errors into account and, therefore, the presented errors of the frequencies correspond only to the statistical errors of fit. The relative frequencies between the lines correspond very well to literature values [25]. We did not find any absolute frequency measurements of the hyperfine spectrum in the literature. As discussed in section 2.2.2, the absolutes frequency values are probably shifted by 0.85 GHz because of an outdated calibration of the wavelength meter.

3.2.2 Repumping from the $6S_{1/2}(F=3)$ to the $6S_{1/2}(F=4)$ State

In contrast to the measurements from the previous section, we now scan the pump laser around the $6S_{1/2}(F=3) \rightarrow 5D_{5/2}(F=1-5)$ hyperfine levels. The laser is still stabilized to the hyperfine transition between the $6S_{1/2}(F=4)$ level and the $6P_{3/2}(F=5)$ level. Hence, the pump laser and the probe laser do not share the same ground state as illustrated in figure 19.

To measure an altered transmission of the probe laser through the cell, the number density of atoms of the $6S_{1/2}(F=4)$ level has to change. The number density of atoms in this state changes when the pump laser excites atoms to the $5D_{5/2}$ state, because these atoms can decay via the $6P_{3/2}$ state to the $6S_{1/2}(F=4)$ level. It is appropriate to say that we repump atoms from the $6S_{1/2}(F=3)$ level to the $6S_{1/2}(F=4)$ level. This counteracts the depumping of the $6S_{1/2}(F=4)$ level due to off-resonant excitation of the $6P_{3/2}(F=4)$ level followed by a decay to the $6S_{1/2}(F=3)$ level. We, therefore, expect a higher number density of atoms in the $6S_{1/2}(F=4)$ level and therefore more absorption of our probe laser. This leads to dips in the transmission spectrum of the probe laser. In the measurement shown in figure 20, we observe these dips with good agreement to theoretical calculations.

For this measurement of the hyperfine-resolved spectrum of the quadrupole line, we scanned the frequency of the pump laser with a triangle function at a frequency of 4 Hz. The peak intensity of this laser in front of the cell was about $I_0 = 16.9 \, \mathrm{W/cm^2}$ without modulation. This should be large enough to saturate all hyperfine transitions of the quadrupole line. The intensity of the probe beam was about $I_0 = 49.5 \, \mathrm{mW/cm^2} \approx 18 I_{\mathrm{sat}}$. We used the $F'=5$ line and the $F'=4$ line to calibrate the frequency axis. The frequency and the intensity of the lines is plotted relative to the $F'=5$ line.

The pump laser excites the atoms via the $6S_{1/2}(F=3) \rightarrow 5D_{5/2}$ E2 transition. To describe this transition, we have to use quadrupole selection rules, namely $\Delta F = 0, \pm 1, \pm 2$. Considering this, we expect to see transitions to the $F'=1-5$ hyperfine levels of the $5D_{5/2}$ state in a hyperfine-resolved spectrum. However, we do not see the $F'=1$ line in our measurement. That is because atoms in this hyperfine level decay via the $6P_{3/2}(F=2)$ back to the $6S_{1/2}(F=3)$ ground state, because these are the only available E1 transitions. Therefore, this is a closed cycle, and the number density of atoms in the probed $6S_{1/2}(F=4)$ level does effectively not change.
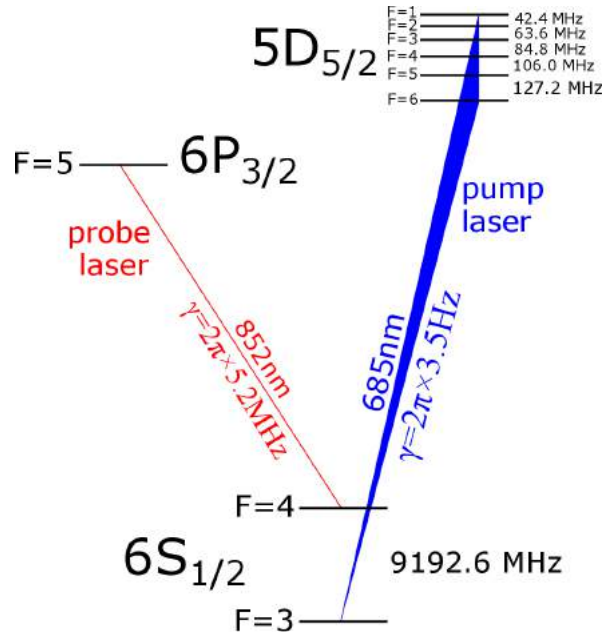
Figure 19: Repumping from the $6S_{1/2}(F = 3)$ to the $6S_{1/2}(F = 4)$ level. The probe laser is stabilized to the same hyperfine transitions as in the previous section. However, now we scan the pump laser across the $6S_{1/2}(F = 3) \to 5D_{5/2}$ E2 transition.

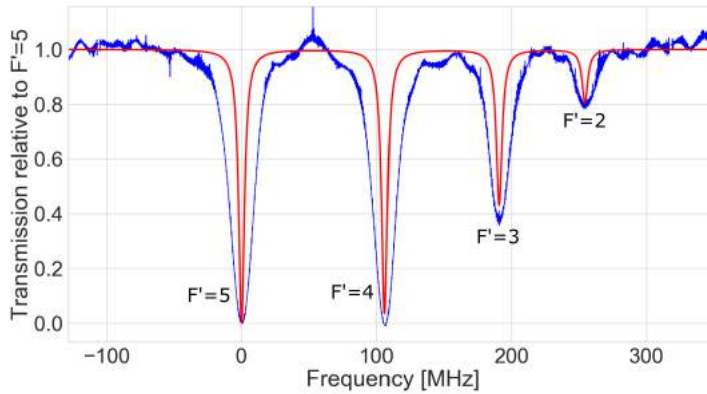Figure 20: Hyperfine-resolved spectrum of the $6S_{1/2}(F = 3) \to 5D_{5/2}$ E2 transition. The frequency and the intensity of the experimental lines are given relative to the $F' = 5$ line. Note that a transmission of 0 does not mean that no probe light is transmitted through the cell. The reason for the increased absorption of the probe laser is that the quadrupole laser repumps atoms from the $6S_{1/2}(F = 3)$ to the $6S_{1/2}(F = 4)$ level. The measured spectrum (blue) agrees very well with our theoretical predictions (red) except for some broadening. As expected, we do not see the $6S_{1/2}(F = 3) \to 5D_{5/2}(F = 1)$ transition.

We use

$$S(F') = -\alpha \sum_{F''} S_{F,F'}^{Q} S^{D}(F', F'') S^{D}(F'', F), \tag{3.6}$$

for the theoretical spectrum shown in figure 20. This equation is similar to equation 3.1 but we removed the first term because the lasers do not share the same hyperfine ground state. Similarly to the last section, we use $\alpha = 0.480656$ since the temperature and the beam diameter did not change. We find an excellent agreement of the relative frequencies and the relative intensities of our measurements with the theoretical predictions. However, the experimental linewidths are again significantly broader than our expectations based on the natural linewidths of the involved states and the frequencies of the lasers (see equation 1.39). As described in the last section, this broadening arises mainly due to power broadening induced by the probe laser.

In the last two sections, we presented two different measurements. We stabilized the probe laser to the hyperfine transition between the $6S_{1/2}(F = 4)$ and $6P_{3/2}(F = 5)$ level and scanned the frequency of the pump laser first from the $6S_{1/2}(F = 4)$ level and then from the $6S_{1/2}(F = 3)$ level over the quadrupole line. It is also possible to lock the probe laser to other hyperfine levels to study the selection rules, the relative line intensities, and the relative frequencies of the lines. This results in similar spectra as presented here.

3.3 Systematic Measurements of the Hyperfine States

In this section, we present systematic measurements of the hyperfine-resolved spectrum of the $6S_{1/2}(F = 4) \rightarrow 5D_{5/2}(F' = 2 - 6)$ E2 transitions to understand the observed amplitudes and FWHMs. We use the same laser settings as in section 3.2.1. The probe laser is stabilized to the $6S_{1/2}(F = 4) \rightarrow 6P_{3/2}(F = 5)$ transition and we scan the pump laser across the $6S_{1/2}(F = 4) \rightarrow 5D_{5/2}(F' = 2-6)$ levels. We will first study the dependence of the experimental spectra on the different powers of the pump and the probe laser. In the last section, we analyze hyperfine-resolved spectra for different AM frequencies.

3.3.1 Role of the Power of the Pump Laser

In the first measurement, we studied the influence of the power of the pump laser on the hyperfine-resolved spectrum of the $6S_{1/2}(F = 4) \rightarrow 5D_{5/2}(F' = 2 - 6)$ E2 transitions. These spectra look similar to the spectrum shown in figure 17. We use Voigt profiles to fit the experimental data. Figure 21 shows the amplitude and the FWHM of these fits, depending on the different intensities of the pump laser.

For these measurements, we scan the pump laser with a triangle function and a frequency of $2\,\mathrm{Hz}$ and used an AM-frequency of $10\,\mathrm{kHz}$ to modulate the pump beam. The probe laser had a power of $100\,\mathrm{\mu W}$, corresponding to an intensity of
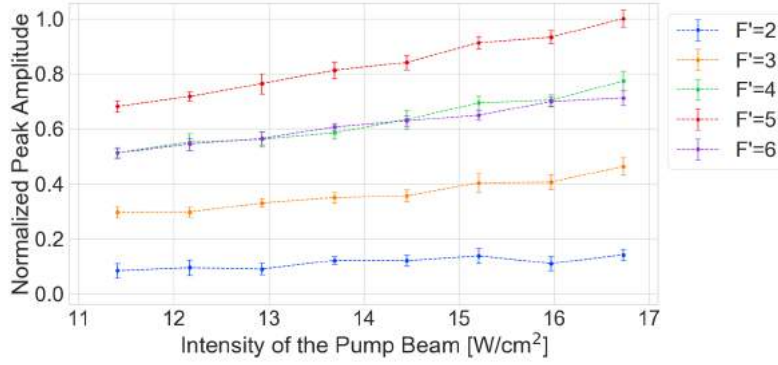
(a)
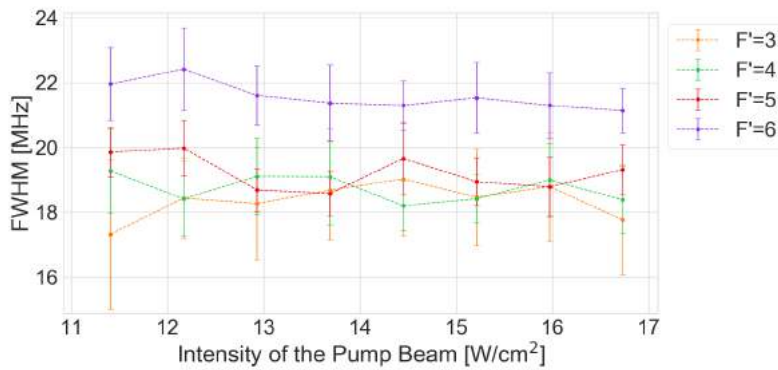
(b)

Figure 21: Hyperfine-resolved spectrum of the $6S_{1/2}(F=4) \rightarrow 5D_{5/2}$ E2 transition for different intensities of the pump laser. We used Voigt profiles to fit the experimental data. The labeling of the lines corresponds to the addressed hyperfine levels of the $5D_{5/2}$ state. (a) shows the amplitudes of these fits. Although the intensities of the pump laser were larger than the saturation intensity, we see that the lines get stronger for higher powers of the pump laser. In (b), we present the FWHMs of the fits. Within the error bars, we see no changes for different powers of the pump laser.

$I_0 = 42.3\,\mathrm{mW/cm^2} \approx 15.6 I_{\mathrm{sat}}$, in front of the cell. We changed the power of the pump laser in integer steps between $15\,\mathrm{mW}$ and $22\,\mathrm{mW}$, which corresponds to intensities between $I_0 = 11.4\,\mathrm{W/cm^2}$ and $I_0 = 16.73\,\mathrm{W/cm^2}$. Since the saturation intensity of the $6S_{1/2}(F = 4) \rightarrow 5D_{5/2}(F' = 2)$ transition is $14.6\,\mathrm{W/cm^2}$, as shown in section 1.1.5, we would expect to see saturation effects of this line. This is the weakest line, and the error is too large to make clear statements about. The other lines are saturated for all pump laser intensities considered here.

We record ten hyperfine-resolved spectra and average them. After averaging, we use the $F' = 6$ peak and the $F' = 5$ peak to convert the time axis into a frequency axis. Then, we fit the experimental data with Voigt profiles. In figure 21(a), the amplitudes of these fits are plotted relative to the maximal amplitude of the $F' = 5$ line. We also fit the hyperfine lines in all ten individually measured spectra. We took the standard deviation of the amplitude of these fits as the error of the fits of the averaged spectrum. The intensities of the pump laser were larger than the saturation intensity for the $6S_{1/2}(F = 4) \rightarrow 5D_{5/2}(F' = 3 - 6)$ transitions. We still see that the lines get stronger for higher powers of the pump laser which is expected in the observed intensity range due to not being much larger than the saturation intensities of the transitions.

In figure 21(b), we present the FWHM of the Voigt fits. The error is again the standard deviation of the fits of ten individual measurements with the same settings. We do not show the $F' = 2$ line because this line is very weak and the error of the FWHM is very large. Within the error bars, the FWHM stays approximately constant. This was to be expected because, in the absence of other broadening mechanisms, the power-broadened FWHM of a transition is [42]

$$\gamma_{\mathrm{S}} = \gamma_0 \sqrt{1 + S_0}, \tag{3.7}$$

where γ_0 is the natural linewidth given by the total decay rate of the state and S_0 is the resonant saturation parameter. S_0 can be calculated with [42]

$$S_0 = \frac{\sigma I(\nu_0)}{\pi \hbar \nu_0 \gamma} = \frac{I(\nu_0)}{I_{\mathrm{sat}}}, \tag{3.8}$$

where the σ is the scattering cross section of the atom, I is the intensity of the laser, and ν_0 is the resonance frequency. Considering power broadening, the linewidth of the $6S_{1/2}(F = 4) \rightarrow 5D_{5/2}(F' = 6)$ transition for an intensity of $I(\nu_0) = 11.94\,\mathrm{W/cm^2}$, as present in our measurement, is

$$\gamma_{\mathrm{SL}} = \gamma_0 \sqrt{1 + \frac{11.94\,\mathrm{W/cm^2}}{0.56\,\mathrm{W/cm^2}}} = 2\pi \times 585.8\,\mathrm{kHz}. \tag{3.9}$$

At the highest intensity $I(\nu_0) = 17.5\,\mathrm{W/cm^2}$, we find a linewidth of this transition of

$$\gamma_{\mathrm{SH}} = \gamma_0 \sqrt{1 + \frac{17.5\,\mathrm{W/cm^2}}{0.56\,\mathrm{W/cm^2}}} = 2\pi \times 704.2\,\mathrm{kHz}. \tag{3.10}$$

Compared to the difference between γ_{SL} and γ_{SH}, our error of the FWHM is too large to measure the power broadening of the pump laser. For technical reasons, we cannot measure larger intensity ranges with our setup which would be necessary to see power broadening of the pump laser.

3.3.2   Role of the Power of the Probe Laser

We now study the effect of the intensity of the probe beam on the hyperfine-resolved spectrum of the $6S_{1/2}(F = 4) \to 5D_{5/2}(F' = 2 - 6)$ E2 transitions. Figure 22 shows these measurements. We scanned the pump laser with a triangle function and with a frequency of $2\,\mathrm{Hz}$ over the quadrupole line and used an AM-frequency of $10\,\mathrm{kHz}$ to modulate the pump beam. We stabilized the probe laser to the transition between the $6S_{1/2}(F = 4)$ level and the $6P_{3/2}(F = 5)$ level and changed the power between $50\,\mathrm{\mu W}$ and $140\,\mathrm{\mu W}$. These powers correspond to intensities between $I_0 = 21.2\,\mathrm{mW/cm^2} \approx 7.8 I_{\mathrm{sat}}$ and $I_0 = 59.3\,\mathrm{mW/cm^2} \approx 21.9 I_{\mathrm{sat}}$.

We averaged ten individually taken measurements and then fitted the experimental lines with Voigt profiles. In figure 22(a), we present the amplitude and in figure 22(b), which is the FWHM of these fits. Similar to the previous section, we do not show the $F' = 2$ peak, because the error is relatively large and we cannot make clear statements about the FWHM of this line. To find the error, we fit the lines of the ten measurements before they were averaged and calculate the standard deviation of the amplitude and the FWHM.

The amplitudes of the lines are shown with respect to the maximum amplitude of the $F' = 5$ line. We find a larger amplitude and a larger FWHM of the experimental lines for higher probe beam powers. The FWHM increases because of power broadening. Considering only power broadening due to the probe laser, we can use equation 3.7 to calculate the FWHM of the lines. Since we change the intensity of the probe beam between $I_0 = 21.2\,\mathrm{mW/cm^2}$ and $I_0 = 59.3\,\mathrm{mW/cm^2}$, we expect the lowest FWHM to be
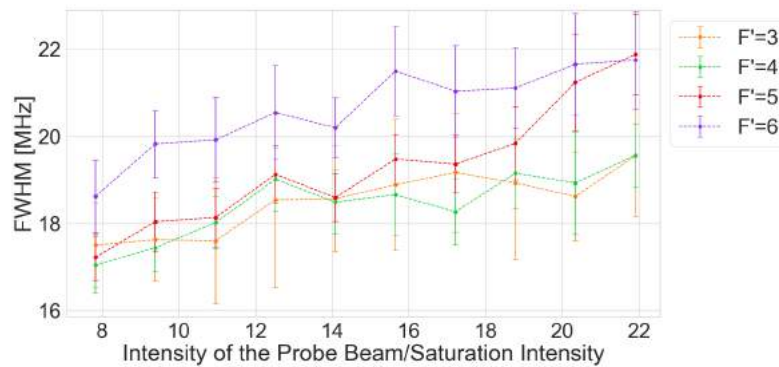
$$\gamma_{\mathrm{SL}} = \gamma_0 \sqrt{1 + \frac{21.2\,\mathrm{mW/cm^2}}{2.7\,\mathrm{mW/cm^2}}} = 2\pi \times 15.5\,\mathrm{MHz}, \tag{3.11}$$

and the highest FWHM to be about

$$\gamma_{\mathrm{SH}} = \gamma_0 \sqrt{1 + \frac{59.3\,\mathrm{mW/cm^2}}{2.7\,\mathrm{mW/cm^2}}} = 2\pi \times 24.9\,\mathrm{MHz}. \tag{3.12}$$
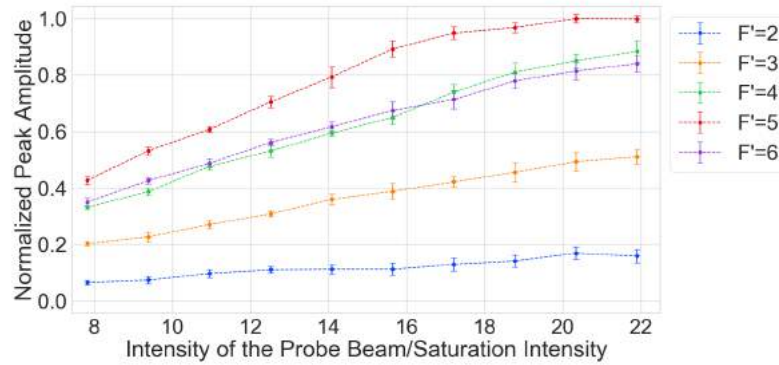
(a)

(b)

Figure 22: Measurements of the hyperfine-resolved spectrum of the $6S_{1/2}(F = 4) \rightarrow 5D_{5/2}$ E2 transition for different intensities of the probe laser. Voigt profiles were used to fit the lines. We used the same labeling as in figure 21. (a) shows the amplitudes of the fits of the experimental lines. We see that the amplitudes get higher for higher intensities of the probe laser. (b) shows the FWHM of the Voigt profiles. Power broadening of the lines is apparent.

For the smallest I_0, the experimentally observed FWHM is larger than what is predicted by equation 3.11. For the largest I_0, the predicted linewidth (equation 3.12) is larger than what is obtained from the measurement. We only take the statistical error of the fit into account. The real error is probably higher and therefore the measured FWHMs probably fit our expectations. However, further studies are necessary to investigate the origin of these deviations.

To measure a FWHM close to the lowest possible FWHM, given by equation 1.39, we would have to use lower probe beam powers. To be able to measure a signal from the probe beam with sufficiently low powers, we would have to use a more sensitive photodiode, or we would have to decrease absorption inside the cell by cooling the cell or using a shorter cell.

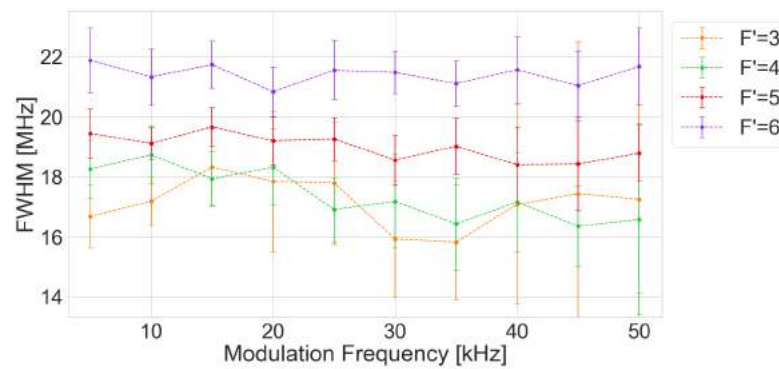### 3.3.3 Effect of the Pump Laser AM Frequency

In this section, we study the effect of the AM frequency of the pump laser on the hyperfine-resolved spectrum of the $6S_{1/2}(F = 4) \rightarrow 5D_{5/2}(F' = 2 - 6)$ E2 transitions. We will discuss the origin of the deviations between theory and expectations of the amplitude of the $F' = 6$ peak in figure 17. In figure 23, we present the fitted amplitude and the FWHM of the measured lines for different AM frequencies. We use the same measurement procedure as in section 3.2.1 to record the hyperfine-resolved spectra. However, now, the probe laser has an intensity of $I_0 = 42.3\,\mathrm{mW/cm^2} \approx 15.6 I_{\mathrm{sat}}$ and the pump laser an intensity of $I_0 = 16.7\,\mathrm{W/cm^2}$ which should be enough to saturate all hyperfine transitions of the quadrupole line.

As described in the previous sections, we use Voigt profiles to fit the peaks in the hyperfine-resolved spectrum. We average ten individually taken measurements before we fit the data. From the fit, we obtain the amplitude and the FWHM of the lines. We also fit the peaks in all ten measurements separately to estimate the error of amplitude and FWHM. We present in figure 23(a) the amplitude and in figure 23(b) the FWHM of the fits as a function of the AM frequency. The FWHM stays constant within the error bars. However, the lines get weaker for higher AM frequencies. This can have two reasons. First, the photodiode which we use to measure the transmission of the probe beam has a bandwidth of about $180\,\mathrm{kHz}$. It was tested experimentally that the hyperfine spectrum cannot be resolved anymore when the AM is performed with a frequency close to the detector's bandwidth limit. This limitation could be overcome by using faster photodiodes. Second, at high AM frequencies, the atomic population cannot follow these fast modulations and the amplitude of the oscillations of the ground state occupation gets smaller which makes the lines weaker.

To simulate this behavior, we use a different notation, as shown in figure 24. We denote the $6S_{1/2}$ ground state, the $6P_{3/2}$ intermediate state and the $5D_{5/2}$ excited state as states 1, 2, and 3, respectively. Three levels are involved in the present measurements
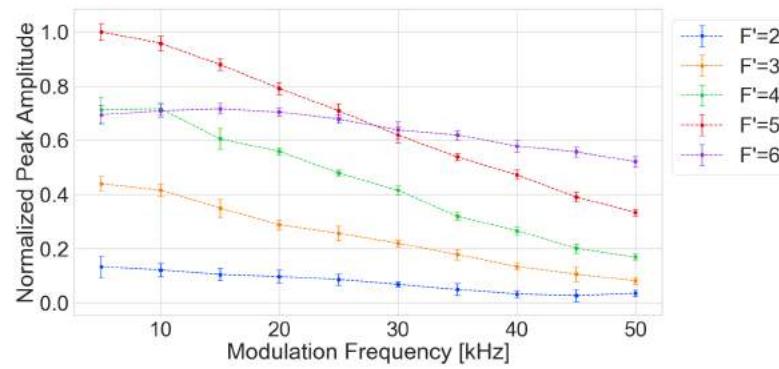
(a)

(b)

Figure 23: Role of the AM frequency of the pump laser. (a) shows the fitted amplitude and (b) the fitted FWHM of the hyperfine levels of the $5D_{5/2}$ state depending on the AM frequency of the pump laser.
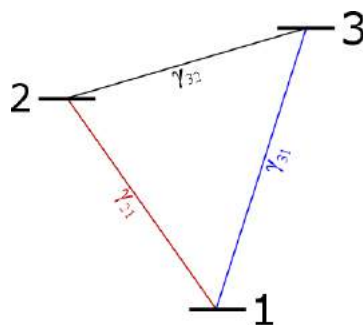

Figure 24: The notation which is used in this section where 1, 2 and 3 correspond to the ground state, the intermediate state and the excited state.

and the following three rate equations can be formulated:

$$\dot{N}_3(t) = -\gamma_{32}N_3(t) - \gamma_{31}N_3(t) + PN_1(t) - PN_3(t), \tag{3.13}$$

$$\dot{N}_2(t) = +\gamma_{32}N_3(t) - \gamma_{21}N_2(t), \tag{3.14}$$

$$\dot{N}_1(t) = +\gamma_{21}N_2(t) + \gamma_{31}N_3(t) - PN_1(t) + PN_3(t), \tag{3.15}$$

where N_i is the number density of atoms in state i and P is a factor which is proportional to the laser power of the quadrupole laser. In figure 25, we study the expected amplitude of the lines for different AM frequencies. We assume that the amplitude is proportional to the peak-to-peak amplitude of the ground state occupation oscillations. We obtain these values by numerically solving the rate equations. We used the literature decay rates in units of $10^6\,\mathrm{s}^{-1}$, presented in section 1.1.4, and an AM laser power of $P = A\sin^2(2\pi\nu_{\mathrm{AM}}t)$, where ν_{AM} is the modulation frequency.
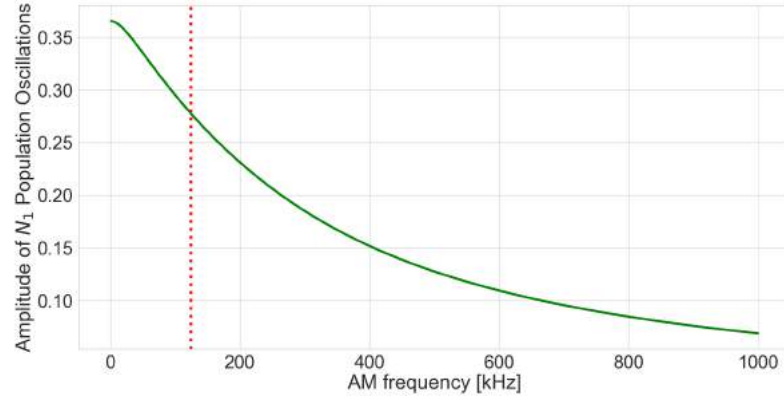
Figure 25(a) shows the population of the three states as a function of time for an AM frequency of $\nu_{\mathrm{AM}} = 50\,\mathrm{kHz}$. For the amplitude of the driving field, we used a value of $A = 1 \times 10^6\,\mathrm{s}^{-1}$. In the beginning, all atoms are in the ground state. Then, atoms get excited to state 3 from where they decay via state 2 back to the ground state. After a settling time, we see constant population oscillations. The peak-to-peak amplitude of the ground state population oscillations is proportional to the amplitude of the peaks in the hyperfine-resolved spectrum. When we study this peak-to-peak amplitude and increase the AM frequency, we see that these oscillations get weaker as shown in figure 25(b). Because the amplitude of the oscillation of the ground state population gets weaker, we expect smaller changes in the absorption of the probe laser leading to weaker lines in the spectrum. This effect arises mainly because of the relatively small total decay rate of the $5D_{5/2}$ state, meaning the populations cannot follow the AM. However, compared to the bandwidth of the photodiode, the decreased oscillation amplitude should play a minor role.

Furthermore, the lower modulation amplitude for high AM frequencies and the low bandwidth of the photodiode cannot explain why the $F' = 6$ peak is getting weaker slower for higher AM frequencies of the pump beam than the other lines. In [9], the hyperfine-resolved spectrum of the $6S_{1/2}(F = 4) \rightarrow 5D_{5/2}(F' = 2 - 6)$ E2 transitions with an AM frequency of $18\,\mathrm{kHz}$ was measured, and no similar effects were described. In contrast to our hyperfine-resolved spectra at this AM frequency, the $F' = 6$ peak is higher than the $F' = 5$ peak.

However, the different behavior of the $F' = 6$ line is probably a result of the different decay channels for atoms in different $5D_{5/2}(F' = 2 - 6)$ levels. For the $F' = 2 - 5$ levels of the $5D_{5/2}$ manifold, atoms can be lost to the $6S_{1/2}(F = 3)$ level. This effect is stronger for low AM frequencies because we have to multiply the amplitude of the ground state occupation modulations with a factor which takes the decay to the $(F = 3)$ level into account. As the probe laser detects changes in the population of
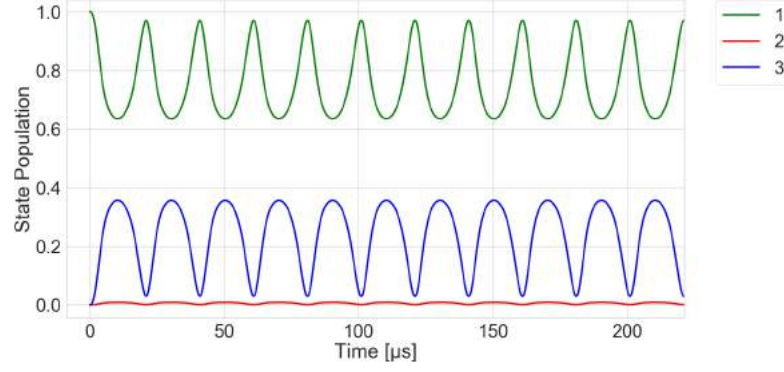
(a)

(b)

Figure 25: (a) shows the population of the involved states for an AM frequency of the pump laser of $50\,\text{kHz}$. In (b), we study the peak-to-peak amplitude of the oscillation of the ground state population after the settling time for different AM frequencies (green). We see that the amplitude gets weaker for higher AM frequencies. This corresponds to weaker peaks in a hyperfine-resolved spectrum of the $6S_{1/2}(F = 4) \rightarrow 5D_{5/2}(F' = 2-6)$ E2 transitions. We note that this effect depends mainly on the low decay rate from the $5D_{5/2}$ state to the $6P_{3/2}$ state $\gamma_{5D6P} = 2\pi \times 124 \times 10^3\,\text{s}^{-1}$ (red).

the $6S_{1/2}(F = 4)$ state, this makes the $F' = 2 - 5$ peaks stronger in the hyperfine-resolved spectrum, especially at low AM frequencies. On the contrary, atoms in the $5D_{5/2}(F' = 6)$ level can only decay via two E1 transitions back to the $6S_{1/2}(F = 4)$ level. This is a closed cycle and no atoms are lost to the $6S_{1/2}(F = 3)$ level. To test this explanation, an additional laser at a wavelength of $\lambda = 852\,\mathrm{nm}$ could be used to repump atoms from the $6S_{1/2}(F = 3)$ level to the $6S_{1/2}(F = 4)$ level. This would lead to higher absorption of the probe laser and, therefore, the $F' = 2 - 5$ lines would get weaker and would probably show the same behavior as the $F' = 6$ line.

3.4   Stabilization on the Quadrupole Line

With the present setup, we can stabilize the laser to the $6S_{1/2} \rightarrow 5D_{5/2}$ E2 transition. This laser is then available for further experiments. We use the measured transmitted power of the probe laser for the stabilization of the frequency of the pump laser to a specific hyperfine transition of the $6S_{1/2} \rightarrow 5D_{5/2}$ E2 transition. As explained in section 2.2, demodulation of a frequency modulated signal results in the derivative of the initial signal. This provides a good error signal for the lock, see section 2.2.1. Figure 26(a) shows the measured hyperfine-resolved spectrum of the $6S_{1/2}(F = 4) \rightarrow 5D_{5/2}(F' = 2 - 6)$ E2 transitions when the pump laser is amplitude modulated with the AOM. In figure 26(b), we apply FM to the pump laser, and demodulation results in the derivative of the AM signal.

In these measurements, we scan the pump laser with a triangle function with a frequency of $5\,\mathrm{Hz}$. The intensity of the pump laser was $I_0 = 16.7\,\mathrm{W/cm^2}$ in front of the cell. We stabilized the probe laser to the transition between the $6S_{1/2}(F = 4)$ level and the $6P_{3/2}(F = 5)$ level. This laser had an intensity of $I_0 = 42.3\,\mathrm{mW/cm^2} \approx 15.6 I_{\mathrm{sat}}$ in front of the cell. To analyze the lock, we stabilize the frequency of the quadrupole laser to the $F' = 5$ line of the spectrum in figure 26(b). In figure 27, we compare the temporal change of the frequency of the unstabilized quadrupole laser to the one locked to the error signal shown in figure 26(b). We measured the frequency of the unstabilized quadrupole laser with the same settings immediately after the measurement of the stabilized quadrupole laser.

We use a frequency of $10\,\mathrm{kHz}$ to frequency modulate the pump beam. We use a home-made PI lock box for the stabilization of the frequency and record the drift of the laser frequency over a $175\,\mathrm{s}$ time interval with a wavelength meter. Compared to the unstabilized quadrupole laser, we note that the stabilization of the laser functions better because the frequency stability is improved significantly. However, the measured frequency of the stabilized quadrupole laser drifts. Long-term drifts of the wavelength meter, arising mainly because of temperature changes, could be one reason. Nevertheless, a good lock is essential for further experiments. In future experiments, the drift will be studied in greater detail to improve the stability.
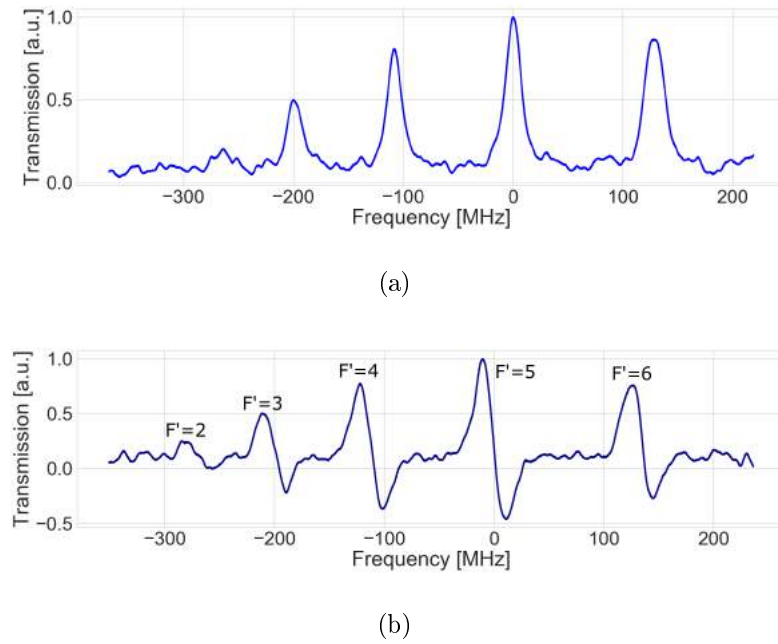
(a)

(b)

Figure 26: In (a), we used AM, and in (b), we used FM to modulate the pump laser. Apart from the modulation, we use the same settings in both measurements of the hyperfine-resolved spectrum of the $6S_{1/2}(F = 4) \to 5D_{5/2}(F' = 2 - 6)$ E2 transitions. Transmission and frequency are in both cases shown relative to the $6S_{1/2}(F = 4) \to 5D_{5/2}(F' = 5)$ transition. We see that the spectrum obtained with FM is the derivative of the spectrum obtained with amplitude modulation.
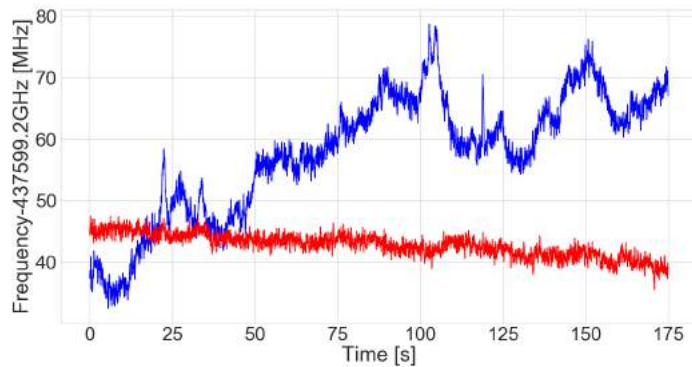

Figure 27: Characterization of the stability of the frequency of the quadrupole laser. We measured the frequency of the quadrupole laser for 175 s with a wavelength meter. The frequency stability of the laser is improved when we compare the stabilized quadrupole laser (red) to the unstabilized quadrupole laser (blue), but we recognize small drifts of the measured frequency of the stabilized quadrupole laser.

Chapter 4

Summary and Outlook

In this thesis, we studied the Doppler-free spectrum of the $6S_{1/2} - 5D_{5/2}$ E2 transition of cesium. The total fluorescence signal, emitted upon excitation of the atoms to the $5D_{5/2}$ state and decay via the $6P_{3/2}$ state back to the ground state, clearly deviated from a Gaussian distribution when scanning the wavelength of a laser over the quadrupole line. This was due to the fact that there are several lines present in the $6S_{1/2} - 5D_{5/2}$ transition. With three-level Raman-type nonlinear spectroscopy, we could resolve this hyperfine structure of the quadrupole line. Among other things, we used this hyperfine-resolved spectrum to analyze the quadrupole selection rules. Studies of the FWHM of the hyperfine transitions of the quadrupole line showed that the widths of the measured lines were broader than expected from calculations. These calculations included the decay rate of the $6P_{3/2}$ state and the wavelengths of the probe laser and the pump laser. One major limitation to the resolution is the probe laser: As shown, the linewidth of the measured hyperfine lines of the $6S_{1/2} - 5D_{5/2}$ E2 transition depends on the linewidth of the transition driven with the probe laser in our case. We stabilized our probe laser to the D2 line of cesium. This transition has a large natural linewidth compared to the natural linewidth of the quadrupole line as illustrated in figure 28.

The large natural linewidth of the D2 line limits the possible resolution of our measurement. To overcome this limitation, one could stabilize the probe laser to the transition between the $6S_{1/2}$ state and the $7P_{1/2}$ state at a wavelength of about $\lambda = 459.44\,\mathrm{nm}$ [52]. The linewidth of this transition is more narrow because the lifetime of the $7P_{1/2}$ state is about $155\,\mathrm{ns}$ [52] which is about fives times longer than the lifetime of the $6P_{3/2}$ state. Probing the $6S_{1/2} - 7P_{1/2}$ transition would yield weaker, but narrower peaks in the hyperfine-resolved spectrum of the quadrupole line. Another possibility to resolve the natural linewidth of the quadrupole line would be to modulate two counter-propagating beams from one laser at different frequencies. When the fluorescence signal is demodulated at the sum frequency, the Doppler-free linewidth can be obtained [47].

Finally, with our setup, we were able to stabilize a laser to the quadrupole line. This makes the setup a useful tool for further experiments. Therefore, this thesis paves the
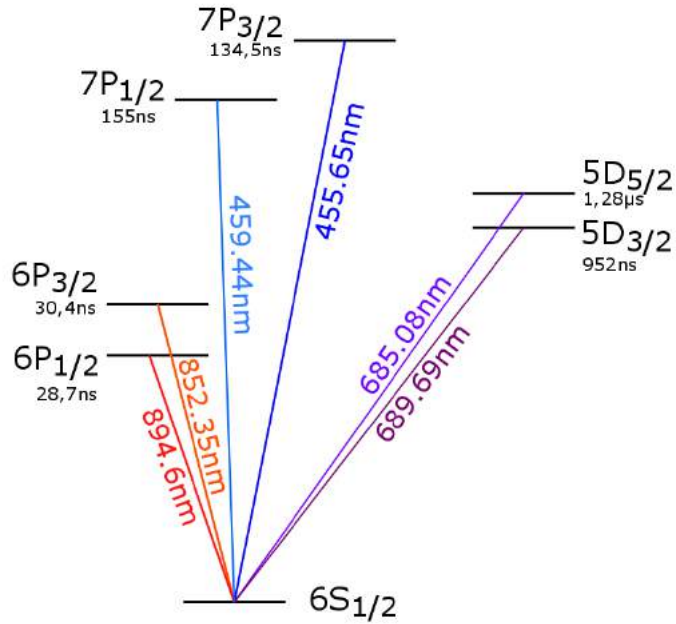
Figure 28: Level scheme of cesium. We used the D2 line at a wavelength of about $\lambda = 852\,\text{nm}$ to probe the number of atoms in the $6S_{1/2}$ ground state. Compared to the lifetime of the $5D_{5/2}$, the lifetime of the $6P_{3/2}$ state is very short. This corresponds to a high natural linewidth of the D2 line which limits the possible resolution of our measurements of the quadrupole line. By probing the transition between the $6S_{1/2}$ state and the $7P_{1/2}$ state at a wavelength of about $\lambda = 459.44\,\text{nm}$, the peaks in the hyperfine-resolved spectrum of the quadrupole line would get weaker but narrower. We took wavelength and lifetime of the $7P_{1/2,3/2}$ states from [52].

way to further studies of E2 transitions. In recent years, the study of E2 transitions of atoms close to surfaces attracted attention. These transitions were theoretically studied for an atom located near a spherical particle of a dielectric and a metal [53–55], near a dimer of spherical particles [56], near an ideally conducting cylinder [57], in optical near fields generated by a subwavelength slit array [58], near an infinite two-dimensional periodic array of core-shell metallic nanoparticles [59], and inside a planar cavity [60]. Furthermore, E2 transitions were theoretically analyzed for atoms close to nanofibers [17]. With trapped, laser-cooled atoms around a tapered nanofiber, it would be possible to study E2 transitions next to surfaces in the presence of the strong field gradient of the evanescent field around the nanofiber. That way, theoretical calculations could be tested. This would help to even better understand the atomic structure and the interaction of atoms with electromagnetic fields.

Bibliography

[1] Mundt A., Kreuter A., Russo C., Becher C., Leibfried D., Eschner J., Schmidt-Kaler F. and Blatt R., "Coherent coupling of a single 40 Ca+ ion to a high-finesse optical cavity", *Applied Physics B*, **76**, 117 (2003)

[2] Schmiegelow C.T., Schulz J., Kaufmann H., Ruster T., Poschinger U.G. and Schmidt-Kaler F., "Transfer of optical orbital angular momentum to a bound electron", *Nature Communications*, **7**, 12998 (2016)

[3] Lembessis V. and Babiker M., "Enhanced quadrupole effects for atoms in optical vortices", *Physical Review Letters*, **110**, 083002 (2013)

[4] Klimov V., Bloch D., Ducloy M. and Leite J.R.R., "Detecting photons in the dark region of Laguerre-Gauss beams", *Optics Express*, **17**, 9718 (2009)

[5] Klimov V.V., Bloch D., Ducloy M. and Leite J.R., "Mapping of focused Laguerre-Gauss beams: The interplay between spin and orbital angular momentum and its dependence on detector characteristics", *Physical Review A*, **85**, 053834 (2012)

[6] Tojo S., Fujimoto T. and Hasuo M., "Precision measurement of the oscillator strength of the cesium $6^2S_{1/2} \rightarrow 5^2D_{5/2}$ electric quadrupole transition in propagating and evanescent wave fields", *Physical Review A*, **71**, 012507 (2005)

[7] Tojo S., Hasuo M. and Fujimoto T., "Absorption enhancement of an electric quadrupole transition of cesium atoms in an evanescent field", *Physical Review Letters*, **92**, 053001 (2004)

[8] Weber K.H. and Sansonetti C.J., "Accurate energies of nS, nP, nD, nF, and nG levels of neutral cesium", *Physical Review A*, **35**, 4650 (1987)

[9] Chan E.A., Aljunid S.A., Zheludev N.I., Wilkowski D. and Ducloy M., "Doppler-free approach to optical pumping dynamics in the $6S_{1/2}-5D_{5/2}$ electric quadrupole transition of cesium vapor", *Optics Letters*, **41**, 2005 (2016)

[10] Nez F., Biraben F., Felder R. and Millerioux Y., "Optical frequency determination of the hyperfine components of the $5S_{1/2} - 5D_{3/2}$ two-photon transitions in rubidium", *Optics Communications*, **102**, 432 (1993)

[11] Ponciano-Ojeda F., Hernández-Gómez S., López-Hernández O., Mojica-Casique C., Colín-Rodríguez R., Ramírez-Martínez F., Flores-Mijangos J., Sahagún D., Jáuregui R. and Jiménez-Mier J., "Observation of the $5p_{3/2} \rightarrow 6p_{3/2}$ electric-dipole-forbidden transition in atomic rubidium using optical-optical double-resonance spectroscopy", *Physical Review A*, **92**, 042511 (2015)

[12] Feld M. and Javan A., "Laser-induced line-narrowing effects in coupled Doppler-broadened transitions", *Physical Review*, **177**, 540 (1969)

[13] Ducloy M., Leite J.R. and Feld M.S., "Laser saturation spectroscopy in the time-delayed mode. Theory of optical free induction decay in coupled Doppler-broadened systems", *Physical Review A*, **17**, 623 (1978)

[14] Thoumany P., Hänsch T., Stania G., Urbonas L. and Becker T., "Optical spectroscopy of rubidium Rydberg atoms with a 297 nm frequency-doubled dye laser", *Optics Letters*, **34**, 1621 (2009)

[15] Vetsch E., Reitz D., Sagué G., Schmidt R., Dawkins S. and Rauschenbeutel A., "Optical interface created by laser-cooled atoms trapped in the evanescent field surrounding an optical nanofiber", *Physical Review Letters*, **104**, 203603 (2010)

[16] Lacroûte C., Choi K., Goban A., Alton D., Ding D., Stern N. and Kimble H., "A state-insensitive, compensated nanofiber trap", *New Journal of Physics*, **14**, 023056 (2012)

[17] Kien F.L., Ray T., Nieddu T., Busch T. and Chormaic S.N., "Enhancement of the quadrupole interaction of an atom with guided light of an ultrathin optical fiber", *arXiv:1709.06700* (2017)

[18] Bartelmann M., Feuerbacher B., Krüger T., Lüst D., Rebhan A. and Wipf A., *Theoretische Physik*, Springer-Verlag (2014)

[19] van der Straten P. and Metcalf H., *Atoms and Molecules Interacting with Light: Atomic Physics for the Laser Era*, Cambridge University Press (2016)

[20] Drake G.W., *Springer handbook of atomic, molecular, and optical physics*, Springer Science & Business Media (2006)

[21] Demtröder W., *Experimentalphysik 3: Atome, Moleküle und Festkörper*, Springer (2005)

[22] Pitz G.A., Fox C.D. and Perram G.P., "Transfer between the cesium $6^2P_{1/2}$ and $6^2P_{3/2}$ levels induced by collisions with H_2, HD, D_2, CH_4, C_2H_6, CF_4, and C_2F_6", *Physical Review A*, **84**, 032708 (2011)

[23] DiBerardino D., Tanner C. and Sieradzan A., "Lifetime measurements of cesium $5d^2D_{5/2,3/2}$ and $11s^2S_{1/2}$ states using pulsed-laser excitation", *Physical Review A*, **57**, 4204 (1998)

[24] Gerginov V., Derevianko A. and Tanner C.E., "Observation of the Nuclear Magnetic Octupole Moment of ^{133}Cs", *Physical Review Letters*, **91**, 072501 (2003)

[25] Fredriksson K., Lundberg H. and Svanberg S., "Fine-and hyperfine-structure investigation in the $5^2D - n^2F$ series of cesium", *Physical Review A*, **21**, 241 (1980)

[26] Steck D.A., "Cesium D line data", available online at http://steck.us/alkalidata (revision 2.1.4, 23 December 2010) (2003)

[27] Eriksson K. and Wenåker I., "New wavelength measurements in Cs I", *Physica Scripta*, **1**, 21 (1970)

[28] Sansonetti C.J. and Andrew K.L., "Spectrum and energy levels of singly ionized cesium: I. Revision and extension of the Cs ii energy levels", *JOSA B*, **3**, 386 (1986)

[29] Rafac R., Tanner C., Livingston A., Kukla K., Berry H. and Kurtz C., "Precision lifetime measurements of the $6p^2P_{1/2,3/2}$ states in atomic cesium", *Physical Review A*, **50**, R1976 (1994)

[30] Chanelière T., Matsukevich D., Jenkins S., Kennedy T., Chapman M. and Kuzmich A., "Quantum telecommunication based on atomic cascade transitions", *Physical Review Letters*, **96**, 093604 (2006)

[31] Roy R., Condylis P.C., Johnathan Y.J. and Hessmo B., "Atomic frequency reference at 1033 nm for ytterbium (Yb)-doped fiber lasers and applications exploiting a rubidium (Rb) 5S 1/2 to 4D 5/2 one-colour two-photon transition", *Optics Express*, **25**, 7960 (2017)

[32] Tanner C., Livingston A., Rafac R., Serpa F., Kukla K., Berry H., Young L. and Kurtz C., "Measurement of the $6p^2P_{3/2}$ state lifetime in atomic cesium", *Physical Review Letters*, **69**, 2765 (1992)

[33] Gerginov V., Tanner C.E., Diddams S.A., Bartels A. and Hollberg L., "High-resolution spectroscopy with a femtosecond laser frequency comb", *Optics Letters*, **30**, 1734 (2005)

[34] NIST, "Atomic Spectroscopy - Spectral Lines", https://www.nist.gov/pml/atomic-spectroscopy-compendium-basic-ideas-notation-data-and-formulas/atomic-spectroscopy (2017)

[35] NIST, "Atomic Spectra Database Lines Form", https://physics.nist.gov/PhysRefData/ASD/lines_form.html (2018)

[36] Hertel I.V. and Schulz C.P., *Atome, Moleküle und optische Physik 1: Atome und Grundlagen ihrer Spektroskopie*, Springer-Verlag (2017)

[37] Steck D.A., "Quantum and atom optics", available online at http://steck.us/teaching (revision 0.12.2, 11 April 2018)

[38] Shore B.W., "The theory of coherent atomic excitation, volume 2, Multilevel atoms and incoherence", *Wiley-VCH*, 1736 (1990)

[39] Varshalovich D.A., Moskalev A.N. and Khersonskii V.K., *Quantum theory of angular momentum*, World Scientific (1988)

[40] Bransden B.H., Joachain C.J. and Plivier T.J., *Physics of atoms and molecules*, Pearson Education India (2003)

[41] Fischer C.F., "Average-energy-of-configuration Hartree-Fock results for the atoms helium to radon", *Atom. Data Nucl. Data Tabl.*, **12**, 301 (1972)

[42] Demtröder W., *Laser Spectroscopy 1 - Basic Principles*, Springer-Verlag Berlin Heidelberg, 5 edition (2014)

[43] Demtröder W., *Laser Spectroscopy 2 - Experimental Techniques*, Springer-Verlag Berlin Heidelberg, 5 edition (2015)

[44] Wieman C. and Hänsch T.W., "Doppler-free laser polarization spectroscopy", *Physical Review Letters*, **36**, 1170 (1976)

[45] Grynberg G. and Cagnac B., "Doppler-free multiphotonic spectroscopy", *Reports on Progress in Physics*, **40**, 791 (1977)

[46] Lamb Jr W.E., "Theory of an optical maser", *Physical Review*, **134**, A1429 (1964)

[47] Sorem M. and Schawlow A., "Saturation spectroscopy in molecular iodine by intermodulated fluorescence", *Optics Communications*, **5**, 148 (1972)

[48] Hoeling B., Yeh J., Takekoshi T. and Knize R., "Measurement of the lifetime of the atomic cesium $5^2D_{5/2}$ state with diode-laser excitation", *Optics Letters*, **21**, 74 (1996)

[49] Schlossberg H. and Javan A., "Saturation behavior of a Doppler-broadened transition involving levels with closely spaced structure", *Physical Review*, **150**, 267 (1966)

[50] Udem T., Reichert J., Hänsch T. and Kourogi M., "Absolute optical frequency measurement of the cesium D 2 line", *Physical Review A*, **62**, 031801 (2000)

[51] Cocquelin B., Lucas-Leclin G., Georges P., Sagnes I. and Garnache A., "Single-frequency tunable VECSEL around the cesium D2 line", in *Solid State Lasers XVII: Technology and Devices*, volume 6871, 687112, International Society for Optics and Photonics (2008)

[52] Ortiz M. and Campos J., "Lifetime measurements of 7P levels of Cs (I) by means of laser excitation", *Journal of Quantitative Spectroscopy and Radiative Transfer*, **26**, 107 (1981)

[53] Klimov V. and Letokhov V., "Increase of spontaneous quadrupole transition rate in the vicinity of a dielectric microsphere", *Optics Communications*, **122**, 155 (1996)

[54] Klimov V. and Letokhov V., "Quadrupole radiation of an atom in the vicinity of a dielectric microsphere", *Physical Review A*, **54**, 4408 (1996)

[55] Klimov V. and Letokhov V., "Effect of the curvature of nanostructures on radiative multipole transition rates", *Comments on Modern Physics*, **2**, D15 (2000)

[56] Guzatov D.V. and Klimov V.V., "Effect of a dimer of nanoparticles on the linewidth of forbidden E2 transitions", *Quantum Electronics*, **46**, 634 (2016)

[57] Klimov V. and Ducloy M., "Allowed and forbidden transitions in an atom placed near an ideally conducting cylinder", *Physical Review A*, **62**, 043818 (2000)

[58] Deguchi K., Okuda M., Iwamae A., Nakamura H., Sawada K. and Hasuo M., "Simulation of electric quadrupole and magnetic dipole transition efficiencies in optical near fields generated by a subwavelength slit array", *Journal of the Physical Society of Japan*, **78**, 024301 (2009)

[59] Yannopapas V. and Paspalakis E., "Giant enhancement of dipole-forbidden transitions via lattices of plasmonic nanoparticles", *Journal of Modern Optics*, **62**, 1435 (2015)

[60] Klimov V. and Ducloy M., "Quadrupole transitions near an interface: general theory and application to an atom inside a planar cavity", *Physical Review A*, **72**, 043809 (2005)

Danksagung

Ich bedanke mich bei allen, die mich während meines Studiums begleitet und unterstützt haben.

Mein Dank gilt insbesondere Univ.Prof. Dr. Arno Rauschenbeutel, der mir die Gelegenheit gegeben hat meine Diplomarbeit in seiner Arbeitsgruppe zu machen. Besonders danken möchte ich Dr. Alexandre Dareau, Dr. Philipp Schneeweiss und Dr. Christoph Clausen, ohne deren hervorragende Betreuung diese Arbeit nicht zustande gekommen wäre und von denen ich sehr viel lernen konnte. Meinem Tischnachbarn Martin, der mir bei Problemen immer zur Seite stand, bin ich auch zu Dank verpflichtet. Danke auch an alle anderen "Fibers" für das hervorragende Gruppenklima.

Darüber hinaus möchte ich noch meinen Studienkollegen (insbesondere: Anja, Christopher, Clemens, Elli, Eva, Florian, Hedwig, Herbert, Johannes, Lea, Manuel, Markus, Nico, Norbert, Paul, Philipp, Sandro und Thomas) dafür danken, dass sie mich immer unterstützt haben und die Studienzeit zu einer sowohl unterhaltsamen als auch erfolgreichen Zeit gemacht haben. Ebenso danke ich meinen weiteren Freunden, die mich während des Studiums immer unterstützt und aufgemuntert haben.

Der größte Dank gilt aber meiner Familie, ganz besonders meinen Eltern, die mir durch ihre Unterstützung das Studium ermöglicht haben und mich immer unterstützt und an mich geglaubt haben.